Volume 61
Number 33
28 April 2025
Pages 6017–6200

ChemComm

Chemical Communications

rsc.li/chemcomm

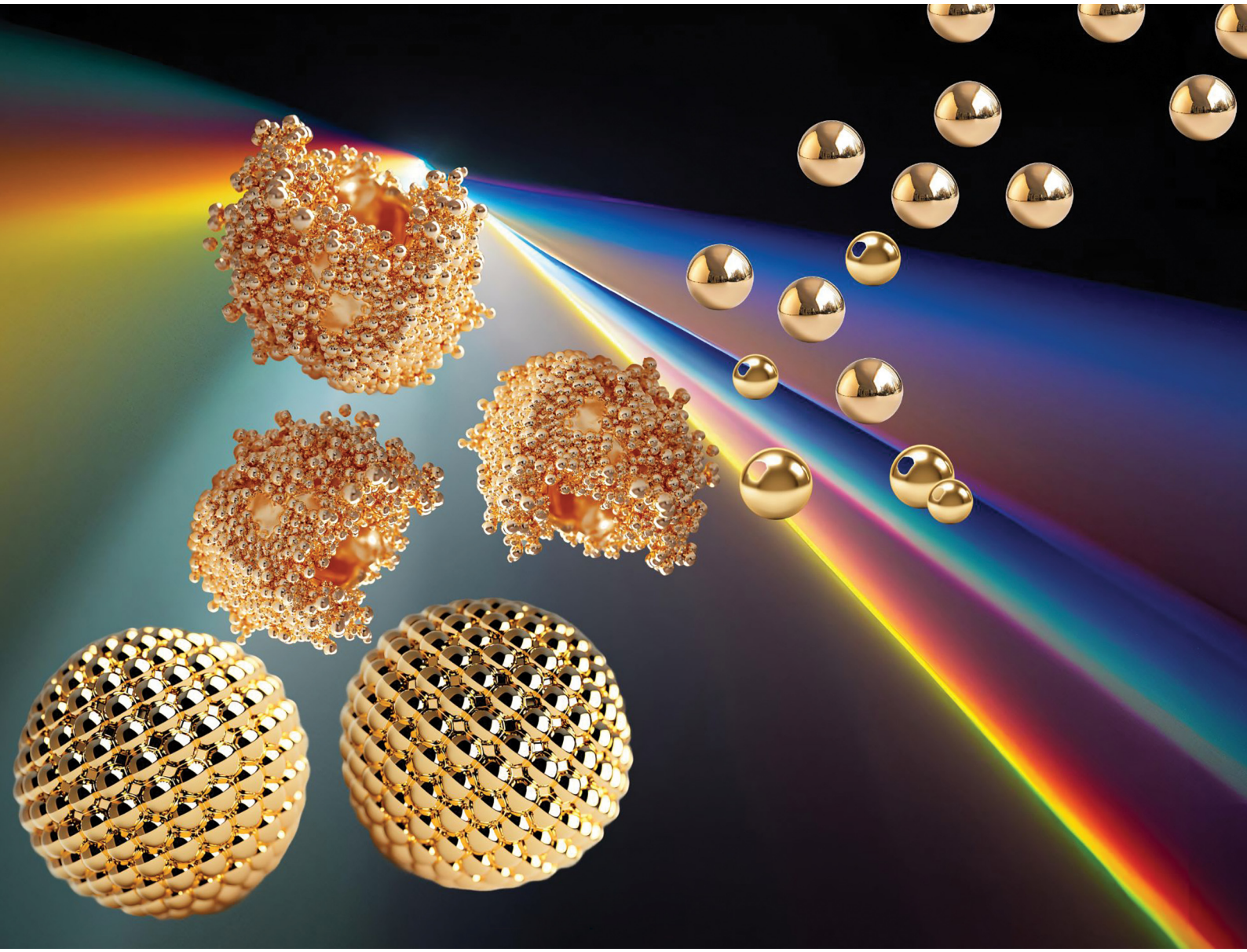

ISSN 1359-7345

ROYAL SOCIETY OF CHEMISTRY

HIGHLIGHT

Deshetti Jampaiah, Suresh K. Bhargava *et al.*
Advances in ammonia decomposition catalysis: a comprehensive analysis of nanoparticle, single-atom, and metal cluster catalysts

ChemComm

HIGHLIGHT

View Article Online
View Journal | View Issue

Cite this: *Chem. Commun.*, 2025, **61**, 6027

Advances in ammonia decomposition catalysis: a comprehensive analysis of nanoparticle, single-atom, and metal cluster catalysts

Pallavi Saini, [a] Deshetti Jampaiah, *[a] Selvakannan Periasamy, [a] Aniruddha P. Kulkarni[b] and Suresh K. Bhargava †*[a]

This review explores the catalytic decomposition of ammonia into hydrogen, a critical process for sustainable hydrogen production. As ammonia rapidly emerges as the preferred carrier for hydrogen storage and transport, efficient decomposition methods are crucial for advancing hydrogen's role in the energy transition. While previously published reviews have primarily focused on metal catalysts such as Ru, Ni, and Co, as well as the influence of supports and other catalytic systems, recent developments in transitioning from nanoparticles to single-atom and cluster catalysts (SACs) have not been extensively covered. Here, we provide a comprehensive analysis of recent advances in the development of nanoparticle, SAC, and metal cluster catalysts—including noble metals, transition metals, and bimetallic systems—for ammonia cracking and their structure–activity relationships. In particular, ruthenium (Ru) remains the standout catalyst due to its exceptional activity and stability. Additionally, it was found that SACs, and metal clusters exhibit remarkable catalytic performance due to their high atom utilization and distinct electronic properties compared to traditional nanoparticle catalysts. This review also discusses the challenges and future opportunities in the field, highlighting the potential of metal catalysts, SACs, and metal clusters to revolutionize ammonia cracking and hydrogen production technologies.

Received 21st February 2025,
Accepted 13th March 2025

DOI: 10.1039/d5cc00953g

rsc.li/chemcomm

[a] *Centre for Advanced Materials and Industrial Chemistry (CAMIC), RMIT University, Melbourne, VIC 3000, Australia. E-mail: jampaiah.deshetti@rmit.edu.au, suresh.bhargava@rmit.edu.au*
[b] *Cavendish Renewable Engineering Ltd., 2/27 Laser Dr, Rowville, VIC, 3178, Australia*
† Senior corresponding author.

1. Introduction

Hydrogen (H_2) is increasingly recognized as a critical component of the future energy landscape due to its high combustion enthalpy of 142 MJ kg^{-1}.[1,2] Its potential as a clean fuel for

Pallavi Saini

Pallavi Saini earned her master's degree in chemistry with honors from Deenbandhu Chhotu Ram University (DCRUST) in 2022. Since 2023, she has been pursuing a PhD at the Centre of Advanced Materials and Industrial Chemistry (CAMIC), RMIT University, under Prof. Suresh K. Bhargava. Her research focuses on developing single-atom and metal cluster catalysts for ammonia decomposition. As an emerging researcher, Pallavi is committed to advancing sustainable catalytic processes and creating innovative materials for industrial applications.

Deshetti Jampaiah

Dr Deshetti (Sampath) Jampaiah earned his master's in chemistry from IIT Madras in 2010 and his PhD in Applied Chemistry from RMIT University in 2016. He worked as a postdoctoral researcher at CAMIC, RMIT (2016–2018) and the University of Antwerp, Belgium, in 2019. Returning to CAMIC in 2020, he became a research fellow in catalysis. His research focuses on catalysts for energy and environmental applications, including CO_2 reduction, ammonia synthesis, and mercury removal. He has authored over 50 publications (h-index 33, 3500+ citations) and three book chapters.

transportation, a versatile energy carrier, and a key feedstock for various industrial processes positions hydrogen as a cornerstone in the transition towards a sustainable and low-carbon energy system.[3–6] Current hydrogen production methods, such as water–gas shift catalysis,[7,8] steam methane reforming (SMR)[9] and water electrolysis,[10,11] have their limitations, including significant carbon dioxide (CO_2) emissions[12] and high energy consumption,[13] respectively. For example, the production of 1 kg H_2 requires 48–55 kW h energy input, which can cause 20–26 kg of CO_2 emissions when considering German power economy[14,15] (470 TW h per annum and 254 Mt_{CO_2} per annum equivalents). Amidst these challenges, ammonia cracking emerges as a promising alternative for efficient hydrogen production.[16] Ammonia (NH_3) cracking has key commercial applications in metallurgy, heavy water production, and stationary and mobile power generation. In metallurgy, ammonia crackers are extensively used as a source of hydrogen for the heat treatment of metals and alloys, particularly for nitriding processes. They are also employed in industrial welding applications. These crackers typically use nickel-based catalysts in packed bed reactors and operate at temperatures between 850–1000 °C. Ni-based ammonia crackers can achieve hydrogen productivity of up to 1500 $m^3\ h^{-1}$ with an efficiency range of 30–60%.[17,18] Heavy water production involves use Co–Fe based catalysts to crack deuterated ammonia at high pressures, producing H_2 and heavy water with productivity up to 425 000 $m^3\ h^{-1}$.[18] Besides these established applications it holds potential for hydrogen refuelling infrastructure, fuel cells for clean energy solutions, and industrial hydrogen supply for chemical synthesis and refining processes. In particularly, Ammonia cracker is being investigated to provide carbon-free hydrogen for alkaline fuel cells, operating below 700 °C with outputs of 5–600 kW.[19,20]

While NH_3 cracking holds immense promise for green H_2 generation, export and transport, its widescale commercialization faces significant hurdles. Key challenges include achieving efficient operation at lower temperatures (below 500 °C) and moderate pressure s to reduce energy costs, enhancing catalytic efficiency with high turnover frequencies and complete ammonia conversion, and ensuring long-term catalyst durability under industrial conditions. Additionally, a seamless integration of ammonia decomposition units with a downstream hydrogen purification and utilization systems, such as fuel cells, remains a critical technical barrier. Overcoming these challenges is essential to make this technology competitive and scalable for industrial applications. Fig. 1 shows a process called on-site NH_3 decomposition H_2 fuelling stations, in which the process can produce highly pure H_2 from liquid ammonia feedstock and further the generated H_2 can be supplied to proton-exchange membrane fuel cell vehicles (PEF-FCVs).

Selvakannan Periasamy

Dr Selvakannan is a Senior Lecturer in Applied Chemistry and Environmental Science at RMIT University, working under Distinguished Professor Suresh K. Bhargava since 2009. His research focuses on CO_2 utilization, methane activation, hydrogen production, endothermic fuels, Raman scattering, and additive manufacturing in catalysis. With 89 publications, 7 reviews, 10 book chapters, and 1 edited book, he holds an h-index of 41. Previously, he was a Research Fellow at the University of Paris-Sud (2007–2009) and a Research Scientist at Tata Chemicals (2005–2007). He earned his PhD (2005) from NCL, India, and chemistry degrees from the American College, India.

Aniruddha P. Kulkarni

Dr Ani Kulkarni is a Materials Technologist specializing in electrochemical and catalytic materials science. With over 22 years of experience, he has advanced electrochemical technologies and membrane reactors from lab to market. He holds an MS and PhD from New Mexico Tech, USA. Dr Kulkarni founded Cavendish Renewable Technology, focusing on industrial decarbonization, and is an Adjunct Professor at RMIT. Previously, he worked at CSIRO, Fortescue Future Industries, Cabot Corporation, and Atlas Copco. He has authored numerous papers and patents and serves on the editorial boards of Frontiers in Chemistry and Frontiers in Energy.

Suresh K. Bhargava

Professor Suresh Bhargava AM is a globally recognized leader in Physical Sciences and Engineering with over three decades at RMIT University. As Founder and Director of CAMIC, he leads a multidisciplinary team pioneering industry-driven solutions. A dedicated mentor, he has supervised 72 PhD students, many now in prestigious roles. His research advances eco-sustainable chemical industries, integrating industry partnerships into academic supervision. A Fellow of eight academies, he has 700+ publications, 350 industrial reports, an H-index of 90, and an i10-index over 500. In 2022, he was awarded the Member of the Order of Australia (AM) for his contributions to research and education.

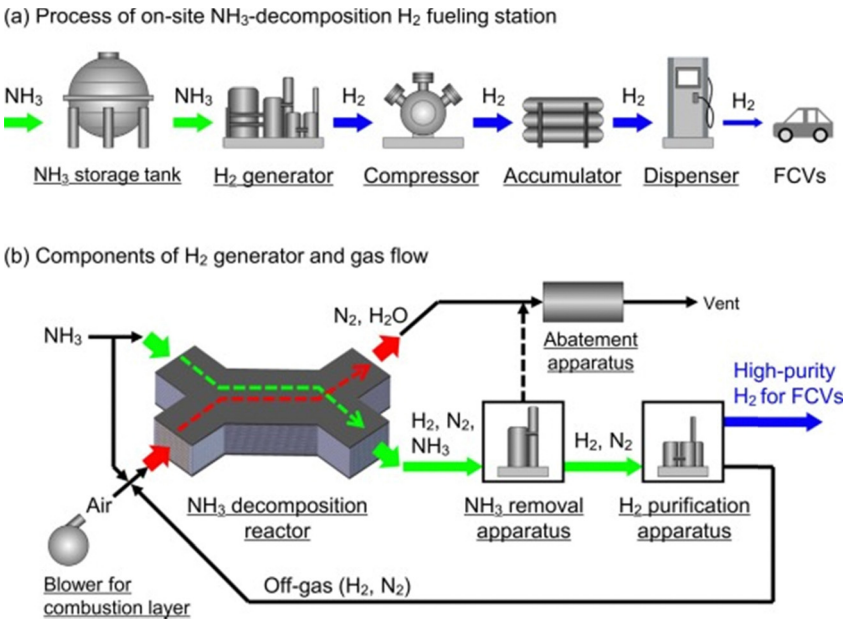

Fig. 1 Schemes of an on-site NH_3-decomposition H_2 fuelling station (a) process of on-site NH_3-decomposition H_2 fueling station and (b) components of H_2 generator and gas flow. (Reproduced from ref. 21. Copyright (2023), with permission from Elsevier).

As mentioned earlier, the primary challenge in utilizing hydrogen lies in its production, storage, and distribution. Typically, H_2 is stored as compressed or liquefied, both of which are energy-intensive, requiring up to 12 kW h of energy per kilogram.[22] Consequently, transport and storage present significant barriers to the commercial-scale adoption of H_2 as a clean fuel. To address these challenges, several H_2 carriers, such as ammonia, methylcyclohexane, green methanol, and other hydrogen derivatives, are being evaluated for storage and transport solutions.

NH_3 is an excellent hydrogen carrier due to its high hydrogen content (17.8% by weight), ease of liquefaction under mild conditions (at −33 °C and atmospheric pressure), high energy density (3000 W h kg^{-1}), and well-established infrastructure for production (Haber–Bosch synthesis), storage, and transportation.[23–25] Moreover, ammonia is carbon free carrier requiring only nitrogen for production in addition to hydrogen, and nitrogen can easily obtained from air using well established air separation technologies.[26,27]

The feasibility of using ammonia as a hydrogen carrier hinges on the development of efficient ammonia cracking technologies as costs associated with ammonia cracking constitutes to about 29% of total Source-to-Tank costs.[28] Ammonia cracking is an endothermic reaction that typically requires temperatures above 670 °C without a catalyst, however, the reaction temperatures can be decreased to under 600 °C in the presence of a catalyst to achieve significant conversion rates.[29,30] The relationship between temperature (250–700 °C) and NH_3 conversion (90–100%) has been shown in various theoretical studies.[31] NH_3 decomposition is temperature-sensitive between 250–450 °C, but conversion rates remain steady above 450 °C. At higher temperatures, the reaction is mainly influenced by kinetic factors, highlighting the importance of understanding kinetic parameters for designing efficient catalytic systems. Several research reports[32–36] indicate that the ammonia decomposition reaction mechanism involves the adsorption of ammonia on the catalyst surface, followed by its dissociation into nitrogen and hydrogen atoms (Fig. 2). These atoms then recombine to form molecular nitrogen and hydrogen, which desorb from the catalyst surface. However, unlike traditional supported metal catalysts, the reaction pathway is different for single-atom catalysts (SACs). Huihuang *et al.*[37] used DFT studies and explained that the recombination of nitrogen (N) atoms to form N_2 follows a pathway influenced by the isolated nature of the active sites. Unlike nanoparticles, which provide contiguous metal sites enabling direct N recombination, SACs rely on alternative mechanisms due to the spatial separation of active sites. If SACs are truly isolated, nitrogen recombination *via* spillover—a process where adsorbed N atoms migrate across the catalyst surface—becomes a critical factor. This mechanism enables N atoms bound to one SAC to interact with those on neighbouring SACs, facilitating N–N bond formation and eventual N_2 release. However, spillover efficiency is dependent on the properties of the support material and the proximity of SACs. In cases where SACs are situated too far apart for effective spillover, recombination may require dual-site activity, often referred to as dual single-atom catalysis. This implies that two neighbouring SACs act cooperatively, allowing adsorbed N atoms on adjacent sites to recombine directly. The role of equilibrium effects is also significant; recombination steps are energetically favourable only if the adsorption and dehydrogenation steps provide sufficient surface N coverage to drive the reaction forward.

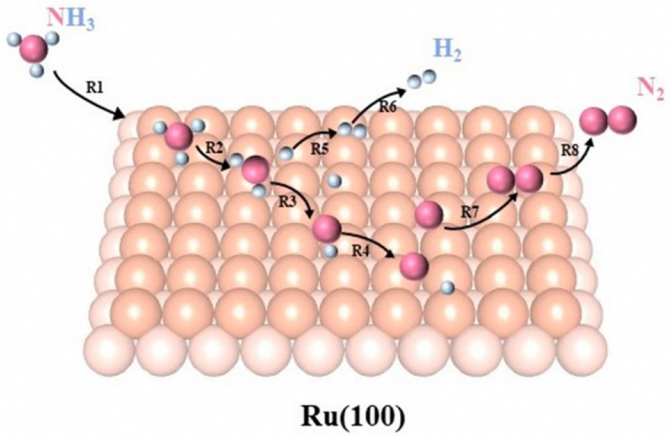

$$NH_{3(g)} + * \rightleftharpoons NH_{3(ads)} \quad (R1)$$

$$NH_{3(ads)} + * \rightleftharpoons NH_{2(ads)} + H_{(ads)} \quad (R2)$$

$$NH_{2(ads)} + * \rightleftharpoons NH_{(ads)} + H_{(ads)} \quad (R3)$$

$$NH_{(ads)} + * \rightleftharpoons N_{(ads)} + H_{(ads)} \quad (R4)$$

$$2H_{(ads)} \rightleftharpoons H_{2(ads)} \quad (R5)$$

$$H_{2(ads)} \rightleftharpoons H_{2(g)} \quad (R6)$$

$$2N_{(ads)} \rightleftharpoons N_{2(ads)} \quad (R7)$$

$$N_{2(ads)} \rightleftharpoons N_{2(g)} \quad (R8)$$

Fig. 2 Reaction pathways of NH_3 decomposition over Ru catalysts. (Reproduced from ref. 38, with permission from Springer Nature, copyright 2020).

Overall, the efficiency and production rate of ammonia cracking is heavily dependent on the choice of catalyst. The ideal catalyst should provide high activity, selectivity, and stability under operating conditions. While various catalysts have been explored, noble metal catalysts have shown particular promise due to their superior catalytic properties.[3,29,39,40] Noble metals, such as ruthenium (Ru),[41,42] platinum (Pt),[43] palladium (Pd),[43,44] and iridium (Ir),[44,45] are known for their exceptional catalytic performance in various chemical reactions, including ammonia cracking.[13,38,39] These metals exhibit high activity and stability, making them suitable candidates for efficient ammonia decomposition. Among them, Ru is considered one of the most effective catalysts for ammonia cracking due to its high activity at relatively low temperatures and strong resistance to sintering and poisoning.[32,38,46]

Most of the reviews discussed the advances in metal catalysts such as Ru, Ni, and Co and the effect of supports and other types of catalysts for ammonia cracking.[3,13,32,34,36,38,39,47,48] However, the recent advances in metal catalysts, and further developments in single-atom catalysts and metal clusters in ammonia cracking reactions are not reviewed extensively. In this review, the recent advances from 2017–2024 in the area of developing different types of metal nanoparticles, single-atom catalysts and their metal clusters such as noble metal, transition metal and bimetallic towards ammonia cracking and the structure–activity-relationship of those catalysts are discussed with a focus on challenges and future opportunities in this field.

2. Thermodynamic and kinetic limitations of ammonia cracking

NH_3 decomposition reaction, mentioned in eqn (1), is an equilibrium reaction with ammonia synthesis as its back reaction. According to eqn (1) ammonia can be decomposed or "cracked" to release hydrogen and nitrogen in a stochiometric ratio of 3 : 1 and it is an endothermic reaction with an overall reaction enthalpy of ΔH_0 = 92.44 kJ mol^{-1}.[14] As mentioned earlier, high temperatures are required for ammonia decomposition due to its endothermicity.

$$2NH_3 \rightleftharpoons 3H_2 + N_2 \quad (1)$$

Fig. 3(a) shows the equilibrium composition of NH_3 and H_2 product as a function of temperature, at constant pressure of 1, 5, and 10 bars, respectively, whereas Fig. 3(b) shows the

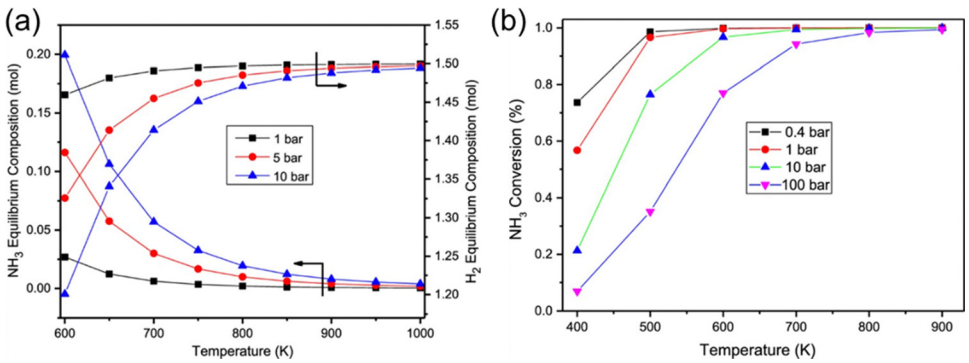

Fig. 3 (a) Equilibrium composition of ammonia and hydrogen product as a function of temperature, at constant pressures of 1, 5, and 10 bars, respectively (MATLAB's minimization of total Gibbs free energy) and (b) conversion of ammonia as a function of reaction temperature at different constant pressures.[14,49] (Reproduced from ref. 49, with permission from Springer Nature, copyright 2020).

ammonia conversions at different pressures including 0.4, 1, 10, and 100 bar, respectively. As shown in Fig. 3(a), it was clear that the ammonia conversion reached almost 100% at temperatures greater than 700 K (427 °C), which indicates that the concentration of ammonia is negligible in the product side. Additionally, the yield of hydrogen from the equation increases as the temperature increases, which agrees with Lechatlear principle.

As shown in Fig. 3(b), the conversion of NH_3 decreases with increasing pressure, in particularly, the changes in NH_3 conversions are obvious at lower temperatures compared to higher temperatures. This is because the kinetics of individual steps are influenced by variables such as temperature, surface coverage of reactants, and the nature of the catalyst material. For example, low-pressure decomposition is suited for applications without high H_2 pressure needs, such as fuel cells in electric vehicles, which operate near atmospheric pressure. This approach minimizes the required decomposition temperature, making it advantageous for compact, mobile heating systems. For large-scale applications, it may also be efficient to keep decomposition temperatures low and compress the hydrogen afterward to moderate pressures.

Conversely, high-pressure ammonia decomposition requires higher reaction temperatures (*e.g.*, >700 °C at 40 bar for >99% hydrogen yield). While this increases energy demands, it may be more efficient for large-scale setups due to reduced reactor volume requirements and the elimination of a separate compression step. The choice between the two pathways hinges on the specific economic and operational needs of the downstream processes.

3. Recent advances in metal nanoparticles for ammonia cracking

The latest trends reflect the exploration of noble and non-noble metal nanoparticles to achieve the overall efficiency and viability of ammonia decomposition. Fig. 4 illustrates the different formulations of metal/support catalysts, which were investigated for ammonia decomposition. Ru-based catalysts are widely regarded as the most efficient for ammonia cracking. Some of the recent reports of highly dispersed metal catalysts including metal nanoparticle, single atom and metal cluster catalysts are summarized in Table 1.

Ru exhibits high catalytic activity, allowing for lower operating temperatures compared to other metals.[36,39] Ru supported on various substrates, such as alumina (Al_2O_3),[88] magnesia (MgO),[37] silica (SiO_2)[89,90] and carbon materials, has demonstrated excellent performance in ammonia decomposition.[3] Pt is another noble metal with significant catalytic activity for ammonia cracking. Pt catalysts, supported on materials like alumina (Al_2O_3)[24] and ceria (CeO_2),[52] show good performance, although they typically require higher temperatures compared to Ru catalysts. Pd catalysts also exhibit good activity for ammonia cracking.[32] Pd-based catalysts are often used in conjunction with other metals or supports to enhance their

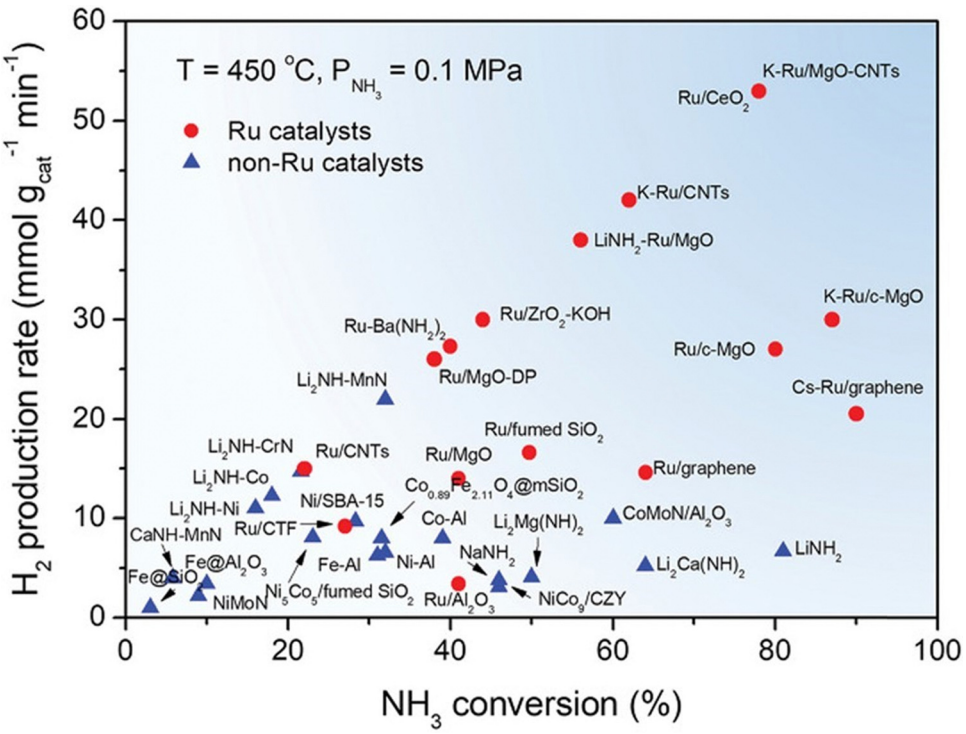

Fig. 4 Performance overview for NH_3 decomposition at 450–600 °C over various types of metal-supported catalysts. (Reproduced from ref. 50, with permission from John Wiley and Sons, copyright 2021). The aggregation states of metal presented in each catalyst are summarized in Table 1.

Table 1 Recent developments of various metal-based catalysts for ammonia cracking

Catalyst	Metal loading (wt%)	Metal aggregation state	Temperature (°C)	Ammonia conversion (%)	NH_3 GHSV (mL g_{cat}^{-1} h^{-1})	r_{H_2} (mmol g_{metal}^{-1} min^{-1})	Ref.
Ru/MgO	3.5	NPs	450	56.5	100 000	893	51
Ru/CNTs	5	NPs	500	84.65	30 000	293	31
Ru/CNTs	5	NPs	350	6.31	30 000	42	31
Ru/CeO_2	1	NPs	450	~70	228 000	9924	52
Ru/CeO_2	1	NPs	350	~35	22 000	814	52
Ni/CeO_2	10	NPs	500	32.6	30 000	114.7	53
Ni/CeO_2	10	NPs	500	20.6	72 000	173.6	53
Ni/Ce/CaNH-HS	10	NPs	500	58.6	30 000	195.6	54
Ru/Y_2O_3	2	NPs	500	86	30 000	1440	55
Ru/MgO	3	Single atom	500	99.8	30 000	1116.7	37
Ru/CeO_2-rods	7	Clusters	500	100	6000	95.7	52
Ru/CNTs	2.5	NPs	500	41	30 000	548	56
Ru/Al_2O_3	2.1	NPs	500	21	30 000	174.5	56
Ru/Al_2O_3	4	NPs	450	~80	12 000	301	57
K-Ru/MgO	3.5	NPs	450	87	36 000	998	51
K-CoNi–MgO–CeO_2–SrO	60	NPs	500	71.9	72 000	96.3	58
$Ru/Ca(NH_2)_2$	10	NPs	400	91	3000	33	59
Ru–Cs/MgO	5	NPs	360	81.5	300	1116.7	59
Nano-RuO_2@SiO_2	—	NPs	500	89.8	30 000	43.2	60
Ru/CrO_3	5	NPs	600	100	30 000	667	61
Ru/CeO_2-nanorods	1	NPs	500	100	22 000	2464	52
Ru/CeO_2-rods	7	NPs	500	100	6000	95.7	62
$Ni–Ce/Al_2O_3$	43.4	NPs	500	63.9	30 000	49.3	63
Ni/5MgLa	10	NPs	500	40.1	30 000	133.9	64
Ru/La_2O_3	4.8	NPs	450	58.2	18 000	304	65
Ni/CeO_2	10	NPs	500	50	6000	33.1	66
Ni/La_2O_3	10	NPs	500	45	6000	30.1	66
$Ni–La/Al_2O_3$	37.9	NPs	500	71.9	30 000	63.6	67
Ru/c-MgO	2.9	NPs	450	75	30 000	890	68
Ru/MgO-DP	5	NPs	500	91	36 000	732	51
Ru/MgO-DP	5	NPs	500	54	100 000	1206	51
$Ru/Ba/ZrO_2$	3	NPs	500	53	30 000	593.3	69
$La_{0.5}Sr_{0.5}NiO_3$-δ-H_2	25.6	NPs	500	42	30 000	55.1	70
Ru-CeO_2NR	0.5	NPs	450	96.1	30 000	2194	46
Ru-CeO_2NR-v	0.5	NPs	450	99.11	12 000	4604	46
$NaNH_2$	—	NPs	450	54.9	—	—	71
$LiNH_2$	—	NPs	450	90.7	—	—	71
90FeAl	90	NPs	600	86	36 000	—	72
90CoAl	90	NPs	600	100	36 000	—	72
90NiAl	90	NPs	600	93	36 000	—	72
Ni/SBA-15	10	NPs	500	49.1	30 000	16.4	73
Fe@SiO_2	—	NPs	550	~60	—	20.3	74
Fe@Al_2O_3	—	NPs	550	~60	—	—	74
$Co_{0.89}Fe_{2.11}O_4$@mSiO_2	3	NPs	450	31.5	22 800	8.02	75
Ni_5Co_5/fumed SiO_2	10	NPs	550	76.8	30 000	25.71	76
$NiCo_9$/CZY	10	NPs	550	91.6	6000	6.13	77
Ru/fumed SiO_2	5	NPs	450	49.7	30 000	16.64	78
CoMo/γ-Al_2O_3	5	NPs	600	99.5	36 000	—	79
Mn-CaNH	—	NPs					80
Ni/SiO_2	10	NPs	450	4.2	—	1.3	45
Ir/SiO_2	10	NPs	450	8.1	—	2.6	45
Ni/CNTs	5	NPs	500	57.64	6000	—	81
Ru-$Ba(NH)_2$	4.4	NPs	400	~40	60 000	8.07	82
CS-Ru/graphene	35	NPs	450	85.8	30 000	28.7	83
Ru/K-ZrO_2–KOH	4.85	NPs	350	44.3	60 000	29.6	84
$LiNH_2$-Ru/MgO	5	NPs	550	~100	60 000	68.3	85
Ru/MgO-poly	2.8	NPs	450	41.3	30 000	493	86
Ru/CTF	2	NPs	450	~70	30 000	—	
K-Ru/CNTs	5	NPs	450	97.3	30 000	32.6	87
Ru/Al_2O_3	5	NPs	450	23.4	30 000	7.8	87
Ru/ZrO_2	5	NPs	450	24.8	30 000	8.3	87
Ru/MgO	5	NPs	450	30.9	30 000	10.4	87
Ru/CNT	5	NPs	450	43.7	30 000	14.6	87
Ru/AC	5	NPs	450	28.7	30 000	9.6	87

performance and reduce the overall cost. Ir, while less commonly used than Ru, Pt, or Pd, also shows promise as a catalyst for ammonia cracking due to its high thermal stability and resistance to poisoning.[33] Furthermore, surface basicity is yet another critical determinant of the catalytic performance. Strong basic sites promote the electron transfer to the metal

catalyst, thereby facilitating the associative desorption of nitrogen atoms. Therefore, to further improve the catalytic activity, researchers often introduce promoters like Na, K, Li, Cs, La, Ca, and Ce.[42] Non-noble metal catalysts such as Ni,[91–94] Fe,[92,95,96] and Co[97,98] on a variety of supports have also been examined for ammonia cracking reactions.

3.1. Noble metal nanoparticles-based catalysts

Based on the literature, noble metals like Ru, Ir, Pt, Rh and Pd are well-known as promising candidates for the ammonia decomposition reaction due to their high activity and selectivity for breaking the strong N–H bonds. Varisli *et al.*[99] studied ammonia decomposition over a Pt (2.5 wt%)-based catalyst on SiO_2 support and found that very low NH_3 conversion (32%) at 550 °C with GHSV of 5100 mL g_{cat}^{-1} h^{-1}. In another study,[100] the performance was compared between Pt (0.5 wt%) and Ru (0.5 wt%)-based catalysts on Al_2O_3 support, and the later was found to be superior, achieving higher decomposition rates (90%) at lower temperatures (~427 °C). Andrea *et al.*[101] studied the ammonia decomposition on Ru/Al_2O_3 and found that 99% cracking at 500 °C. To further identify the best metal catalysts, Ganley *et al.*[44] investigated Al_2O_3-supported different noble and non-noble metals for ammonia decomposition, and it was found that the catalytic activity of these metals varied in the order of Ru > Ni > Rh > Co > Ir > Fe ≫ Pt > Cr > Pd > Cu ≫ Te > Se > Pb. Among all the catalysts discovered to date,[39] the catalytic activity of Ru-based catalysts is known to be superior. Literature studies imply that the Ru-based catalysts are support-dependent, *i.e.*, the catalytic performance can be significantly altered by varying the support properties. A significant proportion of studies have been reported on Ru-based nanoparticles on different catalyst support such as SiO_2,[74,89,102] CeO_2,[52,103,104] TiO_2,[31,105] MgO,[37,38,51,74] carbon-based supports,[31,42,105,106] and zeolites.[91,107]

Ammonia decomposition is structure-sensitive; therefore, the shape of catalyst particles and their size can induce a significant effect. Often, smaller metal crystallite size results in high NH_3 conversion due to their increased surface area to volume ratio, which enriches more active sites for catalytic reactions. In the case of Ru-based catalyst on Al_2O_3 support, Karim *et al.*[57] varied pretreatment conditions to alter the Ru particle size and shape on the support material. They established a direct correlation between the B5 active sites and particle shape and size. It was reported that the density of B5 sites increased with the particle size of up to 7 nm for flat nanoparticles while the maximum turnover occurred in the range of 1.8–3 nm for hemispherical structured particles.

Similarly, Jacobsen *et al.* represented the relationship between the crystal size and the fraction of total atoms present in the crystal (Fig. 5(a)). This observation infers the optimal size of Ru nanoparticles for effective NH_3 decomposition. Therefore, the structure sensitivity is caused by active B5 sites which are highly dependent on the particle shape.[89] As shown in Fig. 5(b) and (c), B5 sites are specific configurations of five Ru atoms where three atoms are present in one layer and two are placed in the layer above. This unique arrangement makes the Ru catalyst highly active for both the dissociation of the N_2 bond and the association of N atoms.[108,109] Further, several researchers were focussed on maximizing the concentration of B5 sites and studied the effect of this on ammonia decomposition. For example, annealing Ru-loaded carbon nanotubes (CNTs) at varying temperatures alters particle size and increases B5 site concentration.[110] Similarly, controlling Ru dispersion on γ-Al_2O_3 and using reduction-calcination strategies have identified an optimal Ru NP size of 2–3 nm for

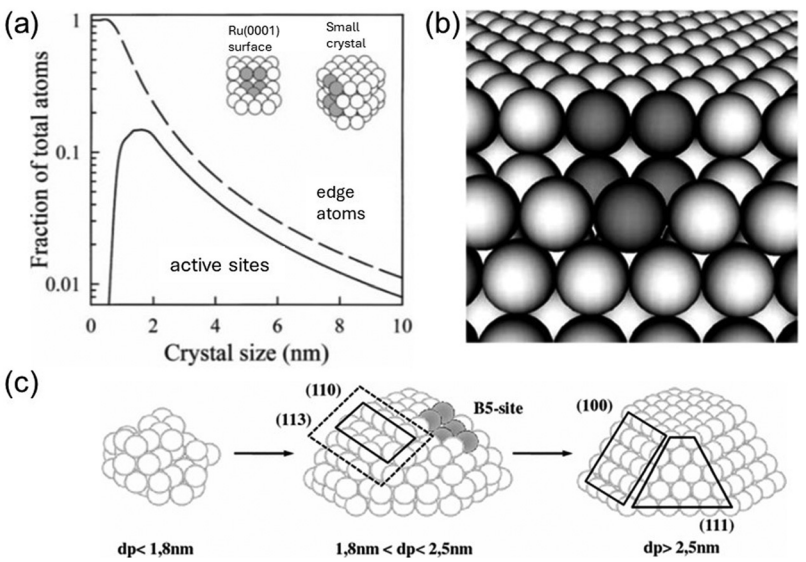

Fig. 5 (a) Three stages of the growth of Ru particle, (Reproduced from ref. 113, copyright (2000) with permission from Elsevier). (b) Schematic diagram of B5 site on Ru(0001) surface (Reproduced with permission from ref. 114, copyright (2008) by the American Physical Society), and (c) fraction of edge atoms and active sites on small Ru crystals relative to the total number of atoms as a function of crystal size. (Reproduced from ref. 115, copyright (2009) with permission from Springer Nature).

hemispherical particles, which maximizes B5 sites.[111] Additionally, elongating flat Ru NPs to ~7 nm *via* metal–support interactions further enriches these sites.[57] Subnanometer Ru clusters confined within MIL-101 frameworks also generate B5 sites due to surface reconstruction.[112] While maximizing B5 sites has been a focus of research, practical limitations arise from synthesis challenges and the complex interplay between particle size, shape, and support interactions. These factors necessitate a balance between maximizing B5 site density and maintaining overall catalytic performance. Therefore, while enriching B5 sites is essential, broader considerations, including catalyst stability, scalability, and cost, often guide research priorities.

Lee *et al.*[89] also reported that the optimal Ru particle size should be <5 nm to achieve maximum activity in the NH_3 decomposition process. Ru/SiO_2 (1 wt%) catalyst calcined at 500 °C and having a particle size of 5.4 nm had shown the highest H_2 production rate of 56 mol_{H_2} mol_{Ru}^{-1} min^{-1} at a GHSV of 60 000 mL g_{cat}^{-1} h^{-1} at 400 °C. Consequently, the particle size of Ru was modulated to achieve the highest performance, and they noted that the particle size can be controlled to some extent by varying the calcination conditions. In a different study conducted by Li *et al.*,[61] the influence of the particle size on the catalytic activity of Ru catalysts was corroborated. The Ru/Cr_2O_3 (5 wt%) has shown the best performance, attaining almost 100% conversion and maximum rate of H_2 generation (30.7 mmol min g_{cat}^{-1}), whereas 1% Ru/Cr_2O_3 (particle size 2 nm) and 10% Ru/Cr_2O_3 (particle size 6 nm) showed 86.7% and 98.9% of NH_3 conversions, respectively. This study suggested optimal size for maximum ammonia conversion is around 4 nm, which closely approximates the dimension of B5-type Ru active sites. Furthermore, the oxygen anions present in the Cr_2O_3 lattice can be potentially replaced by the N atoms and form oxynitrides, increasing the overall catalyst performance towards ammonia decomposition. Therefore, suggesting that the catalytic activity of a catalyst was also influenced by the electronic structure of the support material.

The catalytic activity of the Ru nanoparticles also varies according to the nature of the support material. Huang *et al.*[65] prepared Ru/La_2O_3 catalyst for H_2 production from ammonia decomposition, and Ru/La_2O_3-700-i (4.8 wt%) showed the highest NH_3 conversion of 90.7% at 525 °C with GHSV of 18 000 mL g_{cat}^{-1} h^{-1} outperforming Ru catalysts supported on Er_2O_3, Al_2O_3, SiO_2, and TiO_2. The high catalytic was correlated with the formation of pure La_2O_3 phase and the presence of moderate basic sites on the surface. Ju *et al.*[51] studied a highly active mesoporous Ru/MgO catalyst (3 and 5 wt% Ru loading) synthesised using the deposition–precipitation (DP) method. 5% Ru/MgO-DP catalyst exhibited 100% ammonia conversion and 40.2 mmol g_{cat}^{-1} min^{-1} H_2 formation rate at 550 °C while at a lower temperature (475 °C), the NH_3 conversion was noted at 70.5% and an H_2 production rate of 28.3 mmol g_{cat}^{-1} min^{-1} was observed. They related the surface properties of the supports can play a crucial role in improving the catalytic efficiency, as the support's large surface area and the presence of plenty of macropores not only facilitate uniform dispersion but also ensure mass transfer due to ample active sites.

Modulating the interactions between the Ru nanoparticles and the support material can improve the catalytic performance for ammonia cracking. The metal-support interaction can be enhanced by improving the reducibility of the support material which promotes the formation of oxygen vacancies and forms a strong metal-support interaction (SMSI) resulting in superior catalytic activity. Jeon *et al.*[116] investigated Y-doped $BaCeO_3$ perovskite-supported Ru catalysts by varying Y content (0–20 mol%) for NH_3 decomposition. Fig. 6 demonstrates the SMSI-enhanced NH_3 decomposition over Ru (2.1 wt%) catalyst on Yttrium-doped $BaCeO_3$ support (BCY-x). The content of x equals to the ratio of Y (Ce + Y) ratio. As shown in Fig. 6(a) and (b), it was found that Ru/BCY-10 exhibited the highest NH_3 conversion (48%) compared to Ru/BCY-0 (25%) at reaction conditions of 400 °C, atmospheric pressure and GHSV of 6000 mL g_{cat}^{-1} h^{-1}. Further, the Ru/BCY-10 catalyst was more stable over a 50 h reaction window and maintained 60% NH_3 conversion at 500 °C (Fig. 6(c)). From Fig. 6(d)–(f), it can be seen that the agglomeration of Ru nanoparticles was inhibited in the case of BCY-10 support. It can be concluded that the optimum doping of Y^{3+} and Ce^{4+} into $BaCeO_3$ support played a key role in controlling reducibility and maintaining strong SMSI (Fig. 6(e) and (g)). Overall, Ru particle encapsulation offered by the SMSI shell resulted in the improved long-term stability of the catalyst. The SMSI effects enhance the catalytic activity by generating more active sites at the metal-support interface and altering the electronic properties of nanoparticles. These electronic modifications can significantly influence the adsorption and desorption phenomenon of reactants and the product species, potentially contributing towards long-term stability and ensuring the high dispersion of metal nanoparticles over prolonged use.[117,118]

In conclusion, the choice of support material and tuning the shape and size of the Ru particles can modulate the electronic structure and enhance the metal-support interactions, effectively advancing the activity. Tailoring both Ru catalyst and support is, therefore, a key to improving the catalytic performance, durability, and stability of the material. Moreover, by leveraging the SMSI effects, researchers can design a more efficient and durable Ru-based catalyst for ammonia decomposition.

3.2. Non-noble metal nanoparticle-based catalysts

Non-noble metals particularly transition metals, and their oxides have been widely accepted as highly effective catalysts with outstanding thermal, chemical, and mechanical stability as well as low price.[119–121] The catalytic activity of these transition metals is due to the presence of empty d orbitals, coexistence in different oxidation states, and the tendency to form intermediate complexes which can offer alternative lower-energy pathways for the reaction.[122,123]

Among non-noble metals, Ni-based catalysts have been known to demonstrate high catalytic activity towards ammonia decomposition. Lucentini *et al.*[103] performed a comprehensive

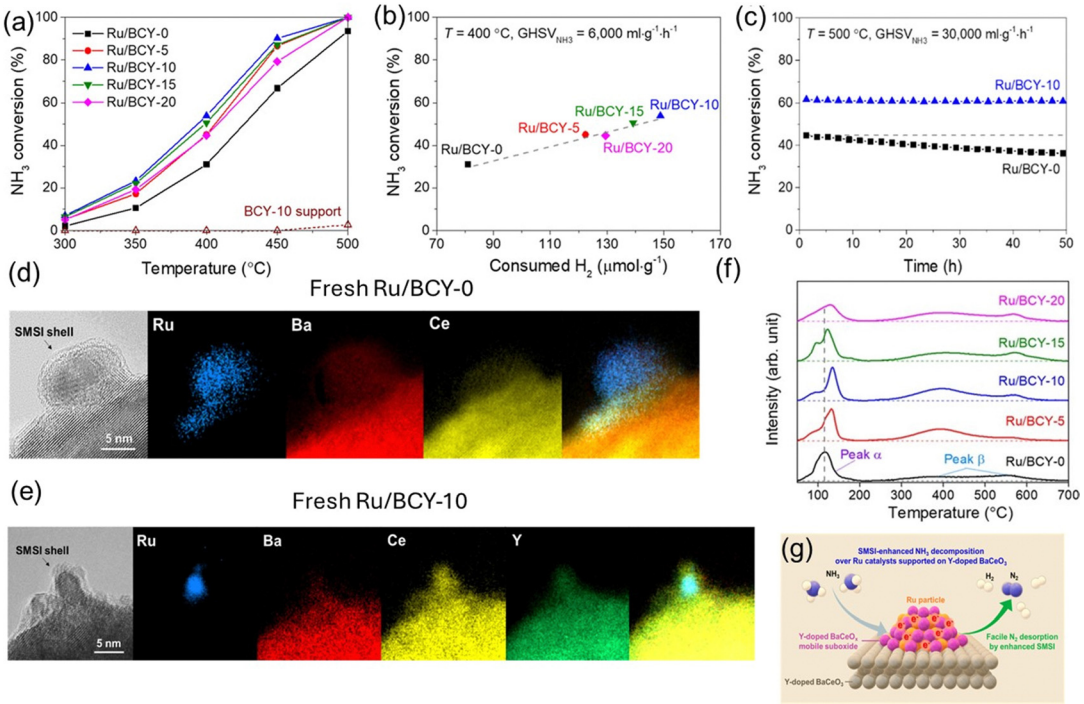

Fig. 6 (a) NH_3 conversion of the Ru/BCY-*x* catalysts and BCY-10 support as a function of temperature (300–500 °C). (b) NH_3 conversion as a function of H_2 consumption for O_L removal during H_2-TPR at 400 °C, $GHSV_{NH_3}$ = 6000 mL g_{cat}^{-1} h^{-1}, and 100 mg of catalyst, (c) long-term stability of the Ru/BCY-0 and Ru/BCY-10 catalysts for a reaction period of 50 h (d) and (e) HR-TEM and EELS mapping images of the prereduced Ru/BCY-0 and Ru/BCY-10 catalysts. NH_3 conversion of the Ru/BCY-*x* catalysts and BCY-10 support as a function of temperature. (f) H_2-TPR profiles of the as-prepared Ru/BCY-*x* catalysts (g) schematic representation of SMSI on NH_3 conversion. (Reproduced with the permission from.[116] Copyright (2022) American Chemical Society).

evaluation of catalytic ammonia decomposition on Ru (2 wt%)/CeO_2 and Ni (10 wt%)/CeO_2 catalysts. A substantial difference existed in the ammonia conversion rates of Ru/CeO_2 (98%) and Ni/CeO_2 (63%) at lower temperatures (450 °C) indicating the superiority of Ru-based catalysts. On the other hand, at higher temperatures (>500 °C), an increased activity as well as stability was noted for Ni/CeO_2. When studied the effect of the support material, they found that CeO_2 outperformed the conventional Al_2O_3. While Ru remains an exception candidate for ammonia decomposition, Ni-based catalysts when paired with optimized support material have emerged to be feasible and cost-effective alternatives.

Previous studies suggested that the catalytic performance of Ni-based catalysts is support-dependent, implying that proper support selection can lead to improved dispersion, resulting in better activity.[74] Various supports such as activated carbons, metal oxides (Al_2O_3, SiO_2, La_2O_3, CeO_2, Sm_2O_3, Gd_2O_3), and mixed-metal oxides ($BaTiO_3$, $SrTiO_3$, $CaZrO_3$, $CeAlO_3$) were used as a support for Ni catalysts and these research works extensively reviewed by Tianxu *et al.*[39] and it was found that the high basicity metal dispersion and larger surface areas are the major factors in enhancing NH_3 conversion. CeO_2 stands out to be an ideal support material, primarily due to its excellent redox and structural characteristics, abundant oxygen vacancies and strong metal-support interactions.[103,124,125] The ability to switch between Ce^{3+} and Ce^{4+} oxidation states facilitates oxygen transfer, promoting ammonia decomposition. Moreover, the surplus oxygen vacancies play a pivotal role in enhancing the catalytic ammonia decomposition by offering more active sites for adsorption and activation of NH_3 molecules.[46] These attributes of CeO_2 make it surpass other conventional supports like Al_2O_3, TiO_2, SiO_2, and carbon-based supports. Even though Al_2O_3 offers good metal dispersion, it falls short in oxygen vacancies and metal-support interactions.[63] Similar to Al_2O_3, SiO_2 supports lack oxygen vacancies and suffer from lower activity and stability compared to CeO_2.[89] Dasireddy *et al.*[126] studied the effect of supports (CeO_2 and TiO_2) on Cu–Zn-based catalysts for ammonia cracking. The Cu–Zn/TiO_2 exhibited lesser ammonia conversion (63%) than Cu–Zn/CeO_2 which showed a catalytic conversion of 79% at 600 °C and was highly stable over the period of 100 h. CeO_2-supported catalysts had better dispersion (16 and 23%), a higher H_2 desorption rate (0.28 and 0.48 μmol g^{-1}), and slightly higher basicity (0.025 and 0.033 μmol_{CO_2} g^{-1}), which collectively contributed toward higher catalytic performance over TiO_2.

Morphologically controlled catalysts offer a high surface area-to-volume ratio compared to conventional nanoparticles, leading to more exposure to active sites available for ammonia decomposition. Tuning the morphology can increase the distribution of oxygen vacancies, enhance electron transfer, control porosity and promote synergism and therefore, promote NH_3 conversion. Recently, Chen *et al.*[127] investigated the

Ni/CeO_2 catalysts of different morphologies (rod(R), sphere (sph), and spindle (spi)) and established that the Ni/CeO_2-R catalyst exhibited the maximum catalytic activity (174.4 mmol of H_2 min^{-1} h^{-1} g_{Ni}) owing to the smaller Ni crystallite size (3.3 nm) and high BET surface area (70 m^2 g^{-1}).[127] Surface acidity and basicity were also the determinant factors of the catalytic properties. Despite the similar sizes of Ni/CeO_2-Sph (5.3 nm) and Ni–CeO_2-Spi (5.3 nm), the latter has high catalytic activity due to the presence of stronger basic sites, attributed to the exposure of CeO_2(110) planes, which showed a high concentration of surface oxygen vacancies. These planes promote nitrogen-associative desorption *via* electron transfer to Ni species. Wu *et al.*[128] designed Ce^{3+}–O–Ni nanostructures with a high concentration of oxygen vacancies through Zr doping and investigated for ammonia decomposition at 600 °C and 30 000 mL g_{cat}^{-1} h^{-1}. It was found that 90% of NH_3 conversion was obtained on $Ni/Ce_{0.8}Zr_{0.15}O_2$ catalyst with 80 h stability. Furthermore, Lucentini *et al.*[125] utilized 3D-printed CeO_2 as support for Ni, demonstrating significantly superior catalytic performance in NH_3 decomposition compared to the conventional cordierite honeycomb support.

By manipulating the synthesis approaches, researchers can achieve control over the morphology, particle size, enhanced metal-support interactions, tailor electronic features and optimize active site distribution, all of which directly influence the catalytic activity. Ulucan *et al.*[94] attempted to explore the structure–property relationship of a MgO-supported Ni catalyst prepared using the wet impregnation (WI) and co-precipitation (CP) approach by examining the influence of synthesis and activation conditions on the Ni nanoparticle dispersion and thereby ammonia decomposition. It can be concluded from Fig. 7(a) and (b) that the Ni/MgO catalysts with 10 and 20% Ni loading prepared by the CP approach resulted in smaller Ni particles (10–20 nm) and showed higher of NH_3 conversion (80–90%) at 550 °C as compared to WI-derived Ni/MgO catalysts which resulted in larger Ni nanoparticles (20–30 nm) and lesser ammonia conversion 70–80%. STEM images in Fig. 7(c) and (d) also validated the small and well-dispersed Ni nanoparticles (4–8 nm) for samples synthesized from CP when compared to WI-derived Ni nanoparticles (7–14 nm). Moreover, the maximum catalytic activity was attributed to the catalyst with higher Ni loadings prepared *via* CP under drastic activation conditions (900 °C in H_2) due to the increased number of active sites (Fig. 7(g)).

As explained earlier in the section on noble-metal catalysts, SMSI can also play a huge role in enhancing the catalytic activity of non-noble metals like Ni. It was reported in several publications that abundant metal-support interfaces could exhibit distinct physical and chemical properties. However, recently, a new approach, which is called inverse structure garnered attention in several catalytic applications such as water–gas shift reactions,[129,130] CO_2 hydrogenation,[131–133] and CO oxidation.[134] This catalyst refers to the small metal oxide nanoparticles supported on large metal particles, which is opposite to the conventional M/M_xO_y catalysts. Based on this approach, Hongawang Liu *et al.*[53] the co-precipitation

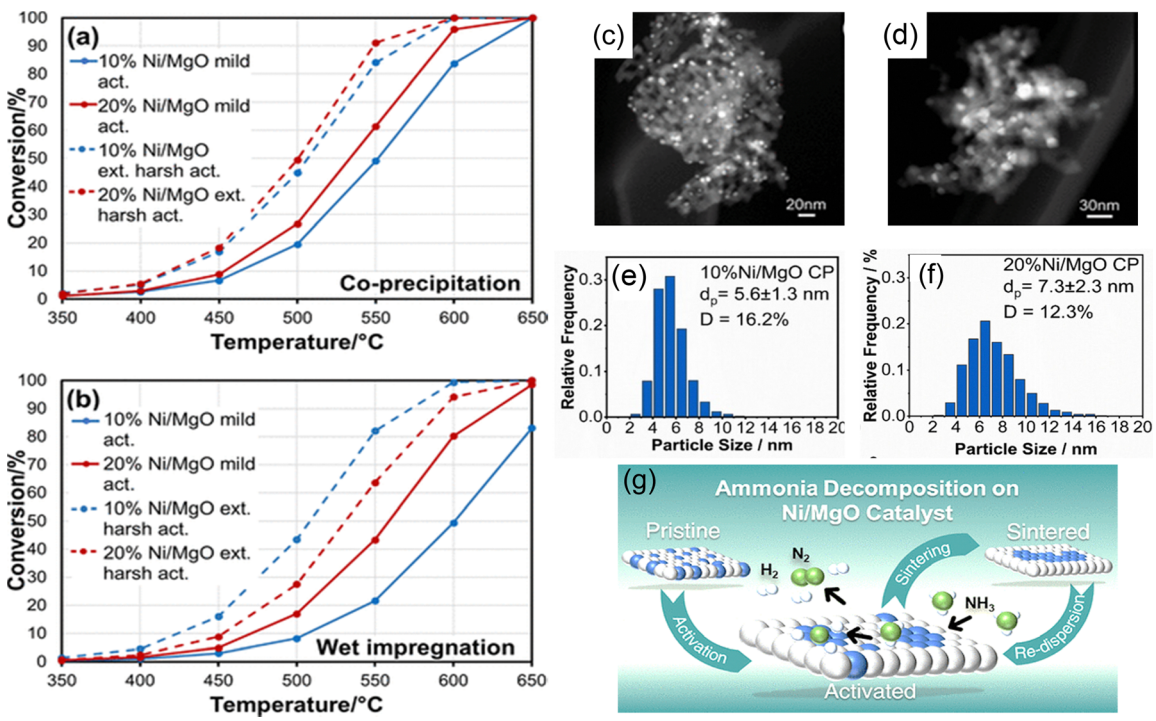

Fig. 7 Catalytic test results of (a) CP and (b) WI samples activated under mild and harsh (external) conditions. NH_3 conversion curves belong to the second decomposition cycle after activation. Representative STEM images of (c) and (d) 10% Ni/MgO-CP (e and f) 20% Ni/MgO-WI activated under harsh conditions with corresponding particle size distribution and dispersion. (g) Schematic view of activation and re-dispersion of Ni sites on MgO support. (Reprinted with the permission from ref. 94 Copyright (2024) American Chemical Society).

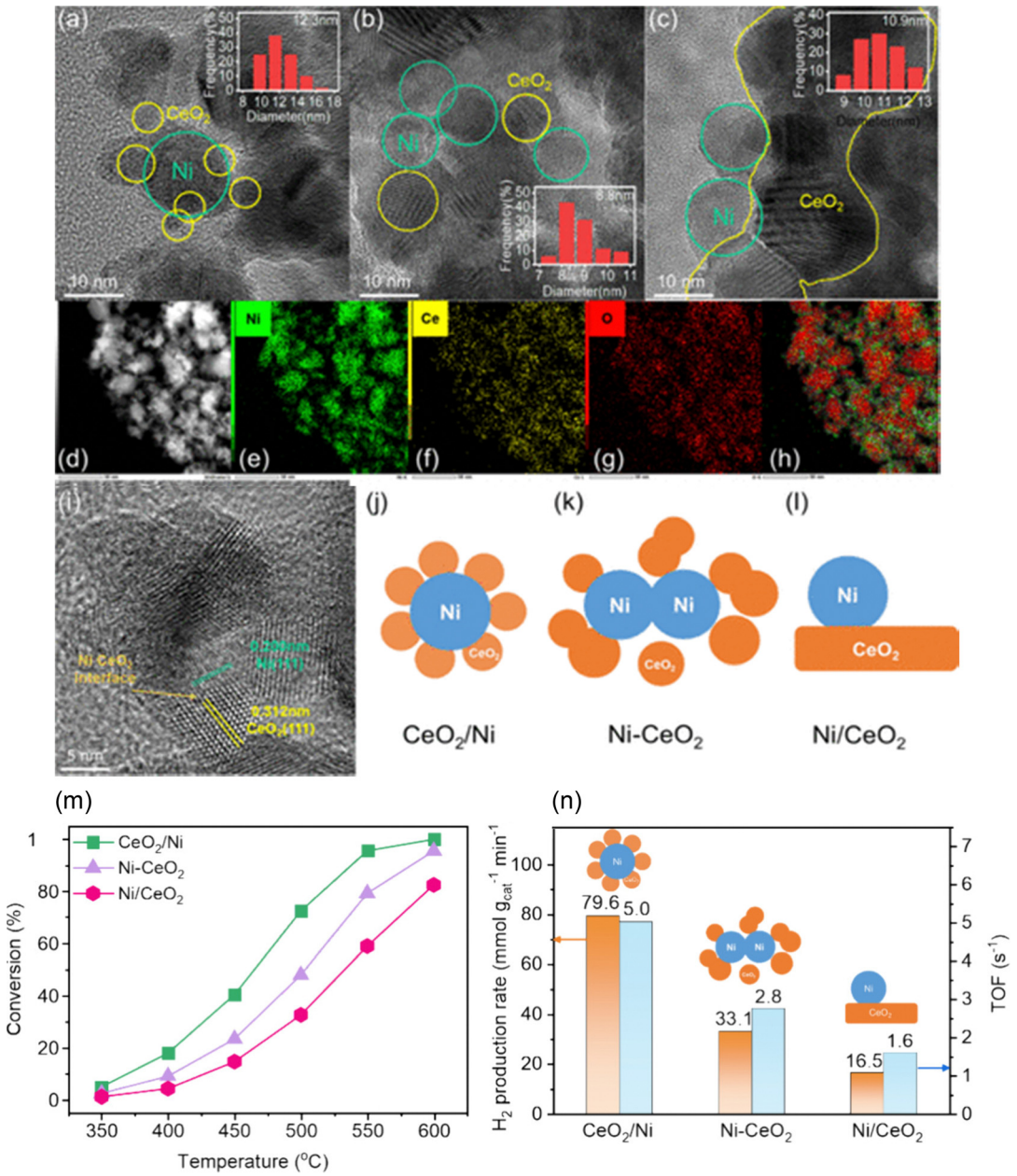

Fig. 8 HRTEM images taken from reduced CeO_2/Ni, (a) Ni–CeO_2, (b) and Ni/CeO_2 (c); yellow circles reflect CeO_2 and green circles reflect Ni. The internal illustration is the size distribution of Ni nanoparticles. (d)–(g) STEM-EDS elemental mapping images of the CeO_2/Ni catalyst. (h) STEM-EDS elemental mapping stacking image of the CeO_2/Ni catalyst. (Green: Ce, red: Ni). (i) HRTEM of the interface and lattice fringes in reduced CeO_2/Ni. Schematic structures of CeO_2/Ni (j), Ni–CeO_2 (k), and Ni/CeO_2 (l). (m) Catalytic performance of NH_3 decomposition over CeO_2/Ni, Ni–CeO_2, and Ni/CeO_2 catalysts *vs.* reaction temperature. GHSV = 30 000 mL g_{cat}^{-1} h^{-1}. (n) Hydrogen production rate and TOF over CeO_2/Ni, Ni–CeO_2, and Ni/CeO_2 catalysts at 500 °C. (Reprinted with the permission from ref. 53. Copyright (2024) American Chemical Society).

methodology to design a highly active and stable CeO_2/Ni inverse catalyst for ammonia cracking and compare the catalytic performance with the conventional Ni/CeO_2. The clear difference between Ni/CeO_2 and CeO_2/Ni can be identifiable from HR-TEM images (Fig. 8(a)–(c)). The yellow circles represent the uniform dispersion of CeO_2 nanoparticles (~5 nm) which are surrounded by Ni nanoparticles whose sizes are around 12.3 nm (blue circle). On the other hand, the smaller Ni nanoparticles (10 nm) interact with the larger-sized CeO_2 nanoparticles. Notably, in the CeO_2/Ni catalysts, STEM-EDS characterization (Fig. 8(d)–(h)) revealed that the Ni nanoparticles were more uniformly enveloped by CeO_2 particles. This suggests a greater number of interfaces in the CeO_2/Ni catalyst compared to the Ni–CeO_2 and Ni/CeO_2 samples. The catalyst featured superior performance for ammonia cracking at 600 °C and exhibited a high hydrogen generation rate of 79.6 mmol g_{cat}^{-1} min^{-1} at 500 °C. The inverse structure promoted the metal-support interactions at the interface which

in turn promoted an increase in oxygen vacancies and active Ni sites, increasing the overall number of adsorption sites responsible for ultimately accelerating the reaction rate.

In another research, Huang *et al.*[97] synthesized cobalt-based catalyst supported on CeO_2 of different morphologies (nanocube (NC) and nanotube (NT)) to evaluate the structure–reactivity relationship for ammonia decomposition. The study suggested that the size-dependent effect of nanoparticles (particle size between 5.2–7.8 nm) is not the main driving factor, but the surface composition/electronic structure of the support strongly influences the catalytic performance. Co/CeO_2 with 3D ordered mesoporous (3DOM) structure has the maximum H_2 production rate (4.2 mmol min^{-1} g_{cat}^{-1}) among Co/CeO_2–NC (3.5 mmol min^{-1} g_{cat}^{-1}) and Co/CeO_2-NT (3.2 mmol min^{-1} g_{cat}^{-1}), owing to its high surface area (90 m^2 g^{-1}) and abundant surface oxygen vacancies. The Co/CeO_2-3DOM (5 wt% Co) catalyst achieved ammonia conversion of 62% at 550 °C and a GHSV of 6000 mL g_{cat}^{-1} h^{-1} as well as demonstrated stability for about 72 hours.

Catalysts for ammonia decomposition often face shortcomings as they become unstable and aggregate at high temperatures. To overcome this, Li *et al.*[135] investigated the effect of core–shell enwrapping of the Fe nanoparticles inside stable microporous and mesoporous silica shells. They attempted to regulate the mass transport during the catalytic process by tuning the porosity of the shell. The nano-Fe-*meso*-SiO_2 showed an 86% of ammonia conversion and hydrogen production rate of 28.76 mmol min^{-1} g_{cat}^{-1} at 600 °C which is a lot higher than 10% Ni/SiO_2 (36.4% ammonia conversion; 11.4 mmol min^{-1} g_{cat}^{-1} rate of hydrogen production). The core–shell catalyst functioned as a microcapsular-like reactor that resulted in more adsorption of the reactant on the core and thus exhibited higher catalytic activity due to the stability of shells (73 hours). Following this they conducted another study[74] on core–shell encapsulated metal nanoparticles ($M@SiO_2$, Al_2O_3, MgO; where M = Fe, Co, Ni, and Ru), it was discovered that all of the obtained catalysts exhibited superior activity for ammonia decomposition and stability than the naked nanoparticles or the supported counterparts. Nano-$Ru@SiO_2$ achieved 100% conversion at 550 °C and H_2 formation rate of 33.5 mmol min^{-1} g_{cat}^{-1} followed by $Ni@SiO_2$ (20.7 mmol min^{-1} g_{cat}^{-1}) and $Fe@SiO_2$ (20.3 mmol min^{-1} g_{cat}^{-1}). The shell surrounding the core, plays a crucial role, creating a microcapsule-like-environment that enhances both adsorption and catalytic efficiency by preventing the agglomeration of the particles.

In conclusion, among non-noble metals, Ni-supported catalysts have emerged as efficient and cost-effective alternatives for ammonia decomposition reaction. Researchers have crowned morphologically controlled CeO_2 as an excellent support material due to its redox and structural features.[136–138] Furthermore, the careful tuning of synthesis approaches has been termed as a crucial aspect for enhancing the catalytic features as it not only enhances the ammonia decomposition reaction but also extends the operational lifespan of the catalyst materials. The holistic approach of encapsulating catalyst nanoparticles in the core–shell structures will provide highly robust and unique environments for catalytic ammonia decomposition by preventing particle aggregation and improving the activity and stability of the catalysts.

3.3. Bimetallic and multi-metallic catalysts

While Ru and Ni-based catalysts are indeed very efficient for ammonia cracking, researchers are now more interested in bimetallic catalysts for multiple reasons that go beyond the performance of monometallic catalysts. Bimetallic and multimetallic alloy compositions generally tend to have superior properties compared to their monometallic counterparts.[139]

Lucentini *et al.*[124] studied Ni–Ru bimetallic catalytic system, and noticed that 2.5 wt% Ni–0.5 wt% Ru/CeO_2 had the best ammonia conversion rate (88.7%) at 450 °C outperforming their individual counterparts by a large extent. The enhanced activity of these bimetallic systems can be attributed to the synergistic effect between different metal nanoparticles where one metal enhances the activity of another metal. Meng *et al.*[140] studied the activity of Fe–Co, Mo–Co, Ni–Fe and Mo–Ni bimetallic catalysts on SiO_2 support along with their monometallic parts for ammonia decomposition. They found the bimetallic 5Fe–5Co catalyst exhibited the best performance and achieved nearly complete NH_3 decomposition (>99.5%) at 585 °C (Fig. 9). The remarkable catalytic activity was attributed to physicochemical characteristics like the nanoparticle size (ranging from 4 to 20 nm), the metal–N binding energy, and the NH_3 adsorption strength. The Fe–Co catalyst demonstrated a high efficiency in activating NH_3 molecules, alongside weak metal–N binding, which is associated with the formation of the FeCo alloy phase. Besides, Simonsen *et al.* established that smaller Ni–Fe nanoparticles are crucial for achieving the optimum catalyst activity.[141,142]

Li *et al.*[143] synthesized a Co–Ni-supported Y_2O_3 bimetallic catalyst using the CP approach. They examined the structure–activity relationship and compared its ammonia decomposition performance with the monometallic $Co–Y_2O_3$ catalyst. The bimetallic $20Co–10Ni/Y_2O_3$ outperformed the $Co–Y_2O_3$ catalyst exhibiting a decomposition rate of 85.02% at 550 °C and a GHSV of 9000 mL h^{-1} g_{cat}^{-1}. This performance was notably superior to monometallic $20Co–Y_2O_3$, showing a 28.5% increase in efficiency and can be attributed to the combination of synergism between Co and Ni and surface properties such as high surface area and the presence of abundant mesopores. Another research[141] discussed the development and optimization of Ni–Fe bimetallic catalysts and explored multiple factors affecting the catalyst performance including the metal loading, particle size, support material, and synthesis approach. They noticed better activity in the case of alloyed $Ni–Fe/Al_2O_3$ than pure Ni/Al_2O_3. Small Ni–Fe nanoparticle sizes were deemed crucial for achieving the optimum NH_3 decomposition due to increased surface area per active site. Al_2O_3 or Mg–Al spinel was considered an ideal support material due to the ease of obtaining small Ni–Fe nanoparticle sizes, in contrast to SiO_2, ZrO_2, and TiO_2 where it became challenging to control the particle size partly due to sintering and reduction of support oxide.

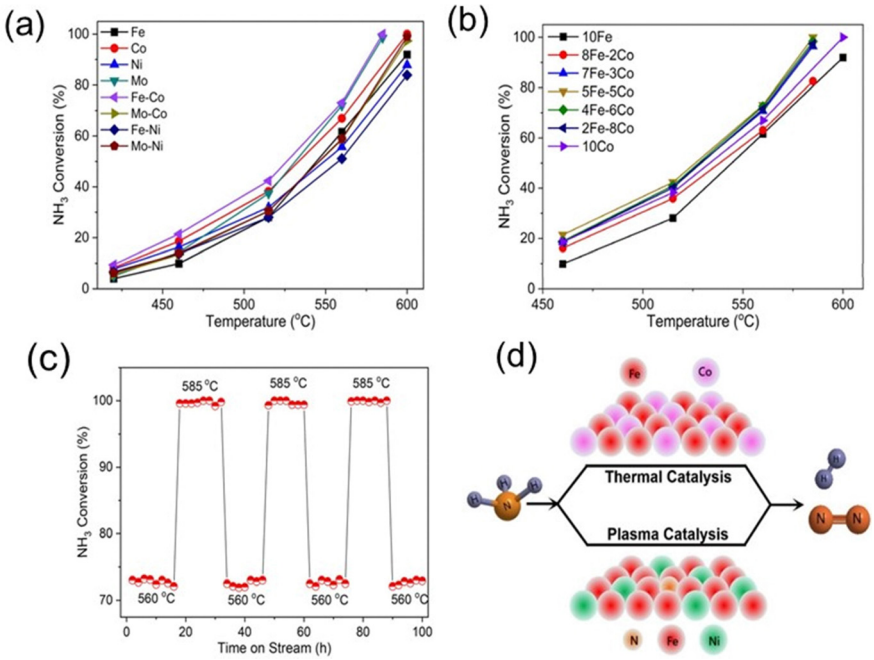

Fig. 9 Results of thermal catalytic NH_3 decomposition. (a) Fe, Co, Ni, Mo, Fe–Co, Mo–Co, Fe–Ni and Mo–Ni catalysts; (b) Fe–Co bimetallic catalysts with varying Fe/Co molar ratios; (c) stability performance of the 5Fe–5Co catalyst. (0.5 g catalyst, 120 mL min^{-1} NH_3, 14 400 h^{-1} space velocity, 3 mm discharge gap, 10 kHz discharge frequency), and (d) schematic representation of the difference between thermal and plasma catalysis. (Reproduced from ref. 140. Copyright (2024), with permission from Elsevier).

Xie *et al.*[144] reported highly efficient high entropy alloy (HEA) multi-metallic catalysts for ammonia decomposition. They synthesized novel CoMoFeNiCu HEA catalyst in a single solid-solution phase using a carbothermal shock technique and found that HEA nanoparticles demonstrated substantially improved catalytic activity (100% conversion at 525 °C) and stability (50 hours of continuous reaction) by an enhancement factor surpassing 20 times that of conventional bimetallic Co–Mo and noble metal Ru catalysts. The HEA nanoparticles formed well-mixed Co–Mo active sites on the surface, consistent with the bulk compositions which likely contributed towards the enhancement of catalytic activity. Moreover, the HEA approach aided in overcoming the miscibility barriers present in traditional bimetallic Co–Mo catalysts, enabling access to more active compositions. The outstanding ammonia decomposition achieved by the HEA can also be attributed to the optimal nitrogen-binding energy achieved in the case of $Co_{25}Mo_{45}$ which facilitated the efficient adsorption of the reactant and desorption of product molecules, maximizing the catalytic performance.

In the context of ammonia decomposition, bimetallic and multimetallic systems have seemingly enhanced the catalytic activity and stability of the catalysts. Research is ongoing to design efficient noble and non-noble metal-based catalysts as they hold significant value for reducing the ammonia production cost by limiting the Ru content. It has been established that bimetallic and multimetallic systems offer multiple advantages over monometallic systems by providing improved conversion rates, greater efficiencies even at lower temperatures due to the increased synergistic effects between the metals.

3.4. Mixed metal oxides

NH_3 decomposition is a support-dependent reaction, and the interaction between the metal and therefore, the choice of support materials is critical in governing the catalytic performance and thermal stability of the catalysts. Researchers have recently explored alternative support materials beyond conventional oxide materials, such as perovskite oxide, carbon nanotubes (CNTs), activated carbons, mixed metal oxide and zeolite materials.

Cao *et al.*[145] modulated the electronic states in the Ru/$La_{1-x}Sr_xAlO_3$ (3 wt%) catalyst by employing the cation substitution. As shown in Fig. 10, the Ru/$La_{0.8}Sr_{0.2}AlO_3$ exhibited superior catalytic activity with 71.6% ammonia conversion and a hydrogen generation rate of 941 mmol g_{Ru}^{-1} min^{-1} at a GHSV of 30 000 mL h^{-1} g_{cat}^{-1}, as a result of electronic metal-support interaction which facilitated the associative desorption of N atom, promoting the ammonia decomposition reaction. Similarly, a balanced cation deficiency strategy was proposed to achieve the maximum ammonia conversion by adjusting the La/Sr ratio in lanthanum strontium titanate nickel perovskite material.[93] The La/Sr ratio was assigned as a critical parameter that controlled the defect chemistry and oxygen transport properties of these perovskite catalysts. A site cation deficiency led to the *in situ* exsolution of Ni particles (Fig. 10) in the B-site of perovskite material was identified as the key reason for the

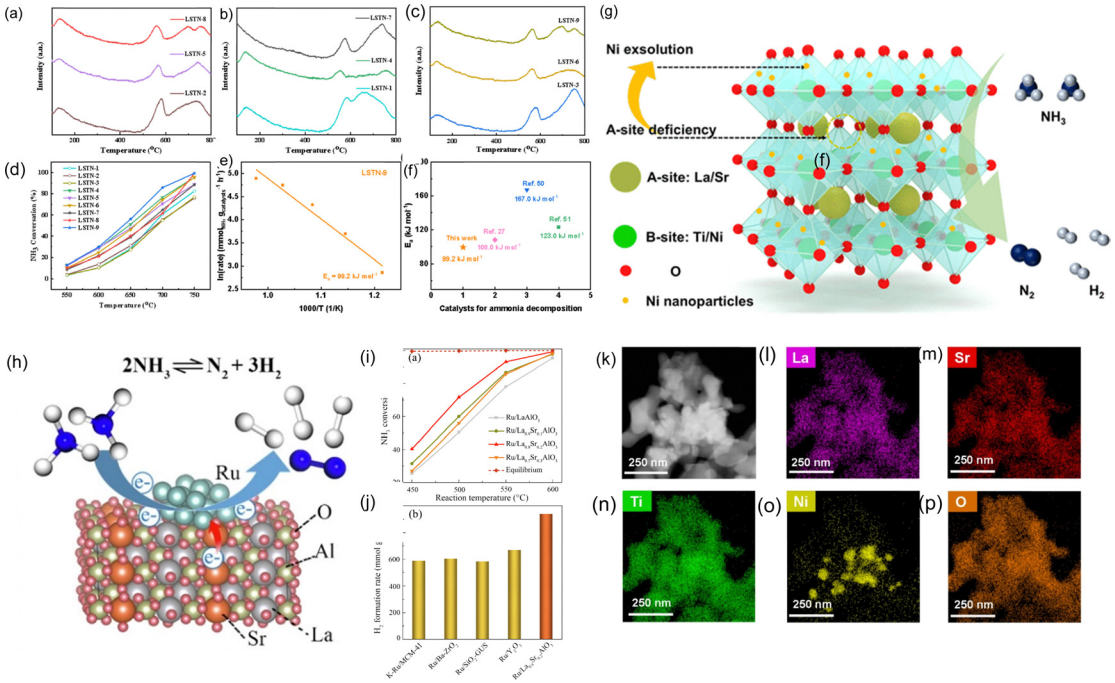

Fig. 10 (a)–(c) NH_3-TPD for LSTN 1–9 perovskite catalysts. (d) Ammonia conversion of LSTN perovskite catalysts. (e) Arrhenius plots for NH_3 decomposition on the LSTN-9 catalyst, showing the apparent activation energy. (f) Comparison of the apparent activation energy of perovskite-derived catalysts in ammonia decomposition reactions. (g) Mechanism of ammonia decomposition Catalyzed by LSTN perovskite catalysts; reproduced with permission from ref. 93. Copyright (2024) American Chemical Society. (h) Schematic illustration of NH_3 decomposition over electron-enriched Ru/$La_{1-x}Sr_xAlO_3$ catalyst; (i) catalytic performance of NH_3 decomposition over Ru/$La_{1-x}Sr_xAlO_3$ (x = 0, 0.1, 0.2, 0.3) catalysts *versus* reaction temperature, where the equilibrium NH_3 conversion ratio was marked by a dashed line. (j) A comparison of the H_2 formation rate over Ru/$La_{0.8}Sr_{0.2}AlO_3$ catalyst (orange column) with those of other Ru-based catalysts (yellow columns) reported in the literature (T = 500 °C). Reprinted with permission from ref. 145. Copyright (2022) Elsevier. (k) Elemental mapping images of the LSTN catalyst and (l)–(p) elemental distribution on the surface of the LSTN perovskite catalyst. Reprinted with permission from ref. 93. Copyright (2024) American Chemical Society.

increased catalytic activity of LSTN9 (85.83% conversion at 700 °C).

In another study, Sima *et al.*[146] reported the enhanced catalytic of Ni/$Ce_{0.8}Zr_{0.2}O_2$ for H_2 production *via* ammonia decomposition. The CeO_2–ZrO_2 composite was found to be highly fascinating due to its positive impacts on the reduction, dispersion, and stabilization of the Ni metal. The Ni/$Ce_{0.8}Zr_{0.2}O_2$ showed an increased ammonia conversion from 48% at 500 °C to 100% at 600 °C at a GHSV of 9000 mL g_{cat}^{-1} h^{-1}. Further doping with an isovalent cation (Al^{3+}) aided in the increased surface area, oxygen defects and catalytic efficiency (complete conversion at 580 °C) due to better Ni dispersion which led to more exposure of B5 sites.

Similarly, Le *et al.*[147] synthesized Ru (2 wt%) supported on the CeO_2–La_2O_3 composite using a DP approach. They found that Ru/$La_{0.33}Ce_{0.67}O_2$ demonstrated a very high catalytic activity (~91.9% of NH_3 conversion at 400 °C with a GSHV of 6000 mL g_{cat}^{-1} h^{-1}). The catalyst exhibited outstanding stability up to 100 hours at 500 °C with a GHSV of 54 000 mL g_{cat}^{-1} h^{-1}. The high catalytic activity of this material was attributed to the strong interaction of Ru with the composite support. The optimal Ce/La ratio of 0.33, offered a right balance between the Ru particle dispersion and support reducibility, leading to the high activity. In another research, the authors reported that the incorporation of La between Ru and Al_2O_3 beads promoted the ammonia conversion. Kim *et al.*[148] reported the synthesis of Ru/Al_2O_3, Ru/$La_2O_2CO_3$, and Ru/$La_2O_2CO_3$–Al_2O_3 beads and found Ru/$La_2O_2CO_3$–Al_2O_3 showed significantly higher activity (80.1% ammonia conversion at 500 °C with a GHSV of 10 000 mL g_{cat}^{-1} h^{-1}) than the other two because the addition of La encourages the electronic interactions between the support surface and the Ru nanoparticles. The strong metal interactions led to higher dispersion (32.2%) of Ru NPs, which increased the number of highly active B5 sites on the surface.

Another class of support material includes layered double hydroxides (LDH) derived mixed oxides, which are generally composed of interchangeable layers of positively charged mixed metal hydroxides and negatively charged interlayer anions. NiMgAl-LDH derived $Ni_x(Mg_yAl_zO_n)$ catalysts with varying ratios of Mg/Ni (0–9) and Mg/Al (0–3) were prepared by Su *et al.*[149] and studied for ammonia decomposition and attempted to study the effects of cation stoichiometry on phase structure. The investigation suggested that the Ni-based catalyst with optimal Mg/Al ratio (= 0.5) exhibited superior catalytic activity (99.3% ammonia conversion at 873 K and H_2 formation of 33.3 mmol min^{-1} g_{cat}^{-1}) compared to Ru catalysts. The catalyst demonstrated a high catalytic activity and stability which was attributed to the structurally isolated active Ni sites and the

synergism between Ni–Mg sites. The hydrogen spillover was identified as a key factor in accelerating the reaction cycles on the Ni active sites.

3.5. Presence of promoters or additives

The introduction of isovalent/aliovalent cations stabilizes the crystallite size, introduces more oxygen vacancies, and enhances the oxygen mobility and ionic conductivity thereby increasing the catalytic activity. In a study,[146] aluminium doping in $Ce_{0.8}Zr_{0.2}O_2$ resulted in a significant increase in Ce^{3+} concentration and the introduction of oxygen defects enhancing the material's catalytic efficiency. A complete ammonia decomposition was achieved at around 580 °C over the Ni/Al–$Ce_{0.8}Zr_{0.2}O_2$ catalyst. The excellent catalytic performance and good stability at 600 °C were attributed to high metal dispersion and abundance of oxygen defect sites, which collectively facilitated more efficient reaction kinetics and stability. The surface oxygen vacancies enhance electron density at the active sites which promotes N atom recombination.

Chen *et al.*[142] studied the effect of Cs promoter on the Ru/C catalyst for H_2 production from ammonia conversion. Different Cs loadings were examined at 350 °C and an increase in ammonia conversion was observed until the Cs/Ru molar ratio reached 4.5 after that the trend reversed due to the increase of transport resistance and electronic conducting resistance. The ammonia conversion almost reached 100% at 400 °C with a GHSV from 48 257 to 241 287 mL g_{cat}^{-1} h^{-1}. The increase in the activity was attributed to the hot ring promotion, where Cs atoms formed a monolayer ring configuration around the Ru crystallite. The effect of different alkaline earth metal promoters (Mg, Ca, Sr and Ba) on Ni/USY zeolite catalyst (10 wt% Ni) was investigated by Cho *et al.*[91] Among them, Mg displayed the maximum enhancing effect on the catalytic activity, because of increased uniform dispersion of Ni nanoparticles and synergism with MgO particles due to acidic and basic properties. S60/1.0Mg/10Ni/USY catalyst presents the maximum ammonia conversion reaching almost 100% around 700 °C, GHSV = 24 000 mL g_{cat}^{-1} h^{-1}.

Moreover, Tabassum *et al.*[58] has reported an alloy type bimetallic CoNi nanoparticles (Co : Ni = 1) supported on Mg, Cs, and Sr mixed oxide with K as a promoter. The catalyst K-$CoNi_{alloy}$–MgO–CeO_2–SrO demonstrated the conversion efficiency of 97.7% and 87.50% NH_3 cracking at GHSV of 6000 and 12 000 mL h^{-1} g_{cat}^{-1}. At 500 °C, the H_2 production rate was almost comparable to that of most Ru-based catalysts. Fig. 11 shows a schematic illustration of homogeneously dispersed CoNi alloy on the mixed oxide support. The HRTEM images depict the overlapping lattice planes of CoNi alloy, highlighting heterostructure formation. Smaller crystallite sizes of approximately 8.7 nm and uniform dispersion of metal nanoparticles increase the number of active sites available for catalysis. The synergistic interactions between CoNi alloys and the metal oxide support enhance the dispersion and improve the stability.

Liu *et al.*[151] examined the effect of alkali metal (KOH) as the promoters for Ru/CeO_2 catalyst. It was found that 5 wt% Ru/CeO_2-NP(KOH) catalyst exhibited 96.6% ammonia decomposition efficiency at 500 °C and GHSV of 30 000 mL h^{-1} g_{cat}^{-1}. The H_2 production rate for Ru/CeO_2-NP(KOH) was 33.48 mmol g_{cat}^{-1} min^{-1}, while for Ru/CeO_2-NP(NH_3) it came out to be 26.8 mmol g_{cat}^{-1} min^{-1}. The K-promoted catalyst exhibited 16.7% higher ammonia production performance than the unpromoted catalyst. It was proposed that the K promotion effect (K serving as an e^- donor for both CeO_2 and Ru active sites) and increased oxygen vacancies were the factors likely to contribute towards the higher efficiency for ammonia decomposition in the former catalyst.

Okura *et al.*[150] attempted to study the effect of alkaline earth metals (Mg, Ca, Ba and Sr) on Ni/Y_2O_3 catalysts (40% Ni loading). They found Mg and Ca to be less effective for ammonia conversion than the unmodified Ni/Y_2O_3 catalyst (63% conversion). On the contrary, 5 wt% SrO–40 wt% Ni/Y_2O_3 and 5 wt% BaO–40 wt% Ni/Y_2O_3 achieved around 81% and 75% ammonia conversion at 500 °C respectively (as shown in Fig. 11). The remarkable improvement in the ammonia decomposition can be attributed to the strong interaction between the Ni and Sr/Ba which led to the formation of composite oxides during calcination while Mg and Ca existed as just MgO and CaO. The stability of 5 wt% SrO–40 wt% Ni/Y_2O_3 was tested sat reaction conditions: 100 vol% NH_3 and W/F = 0.18 g s cm^{-3}, and it showed a remarkable stable over a period of 50 hours (Fig. 11(i)).

In conclusion, extensive research has been carried out on developing catalysts having high efficiency for ammonia decomposition, with Ru being the most studied among the noble metals and Ni in the case of non-noble metal-based catalysts. Studies have revealed that the superiority of these catalysts can be significantly enhanced by incorporating strongly basic elements such as alkali (*e.g.*, Na and K) and alkaline earth metals (*e.g.*, Mg, Sr and Ba). These additives are known to enhance the ammonia decomposition reaction by facilitating the electron transfer process between these basic additives and the surface of the active metal, which promotes nitrogen release at relatively lower temperatures. Hence, the addition of these promoters to the catalyst becomes an excellent choice for improving the catalyst's performance for ammonia decomposition reaction.

4. Single-atom and cluster catalysts for ammonia cracking

The development of novel metal catalysts and the modification of traditional supports have played a significant role in advancing metal-based catalysts for ammonia cracking. As shown in Fig. 12, a particularly innovative approach involves the use of single-atom catalysts (SACs) for ammonia cracking for their maximum atom efficiency and excellent ammonia conversion and mainly the key benefits such as high activity, selectivity, and tuneable interactions between metal atoms and supports. Individual metal atoms and small metal clusters, composed of only a few atoms, exhibit unique catalytic properties influenced

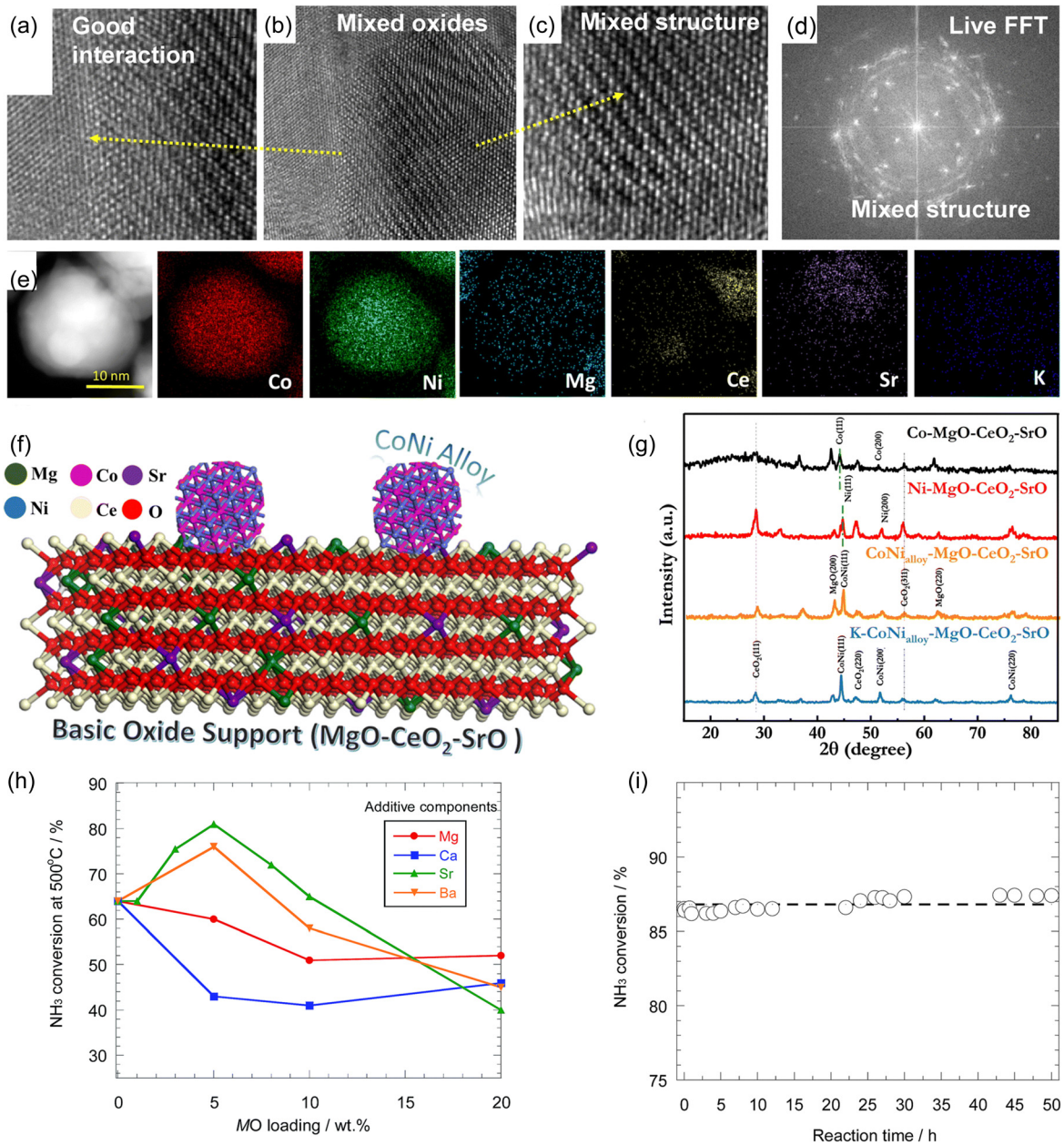

Fig. 11 (a)–(c) HRTEM of overlapped lattice planes of the heterostructure of K–$CoNi_{alloy}$–MgO–CeO_2–SrO catalyst, (d) FFT of the respective mixed heterostructure, (e) HADF-STEM mapping of K–$CoNi_{alloy}$–MgO–CeO_2–SrO along with elemental mapping, (f) schematic illustration for the decorated $CoNi_{alloy}$ on the oxide support of MgO–CeO_2–SrO, and (g) XRD pattern of K–$CoNi_{alloy}$–MgO–CeO_2–SrO and comparative catalysts; (h) ammonia conversion at 500 °C for 0–20 wt% MO–40 wt% Ni/Y_2O_3 catalyst (M = Mg, Ca, Ba and Sr); (i) stability test for 5 wt% SrO–40 wt% Ni/Y_2O_3 at 550 °C. (Reproduced with permission from ref. 58 and 150 from the Royal Society of Chemistry).

by the specific nature of the active metal species. Even minor changes in the active centres can significantly decrease catalyst efficiency, as seen with noble metals like platinum, which can become irreversibly deactivated through sintering under extreme conditions.[152] Supports such as carbon materials, metal oxides, and metal amides are critical in controlling metal particle size, dispersion, and electron density. For example, the use of carbon supports with tailored surface functional groups has been shown to enhance metal-support interactions and improve catalyst stability. Similarly, metal oxides like MgO, Al_2O_3, and CeO_2 have demonstrated promising activity in ammonia decomposition by facilitating strong metal-support interactions. Depending on the orientation of single atoms, mostly they are classified as a noble metal and non-noble metals. Further, the single-atom catalysts can aggregate into clusters or larger nanoparticles depending on various reaction conditions such as high temperature or reductive atmospheres. Further discussion related to these systems is critically evaluated in the following sections.

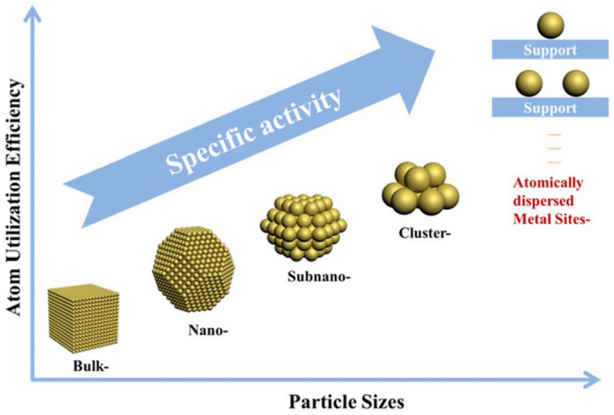

Fig. 12 Schematic diagram of the research on multi-scale and corresponding activity presented in this review. (Reproduced from ref. 153. Copyright (2022), with permission from Wiley).

4.1. Noble metal single-atom catalysts

Ruthenium (Ru) has long been recognized as one of the active metals for both synthesis and decomposition of NH_3 under mild conditions.[32,35,47] Although Ru-based catalysts show significant ammonia conversion, however, the landscape has changed dramatically in recent years, with the market price of Ru increasing substantially. This has spurred ongoing research aimed at achieving cost-effective and sustainable use of Ru in catalytic applications. Therefore, the initial cost of these catalysts can be greatly lowered by utilizing single-atom catalysts. SACs offer maximum atom efficiency, as every atom is actively involved in individual catalytic reactions.

Fang *et al.*[37] prepared single-atom Ru catalysts deposited on MgO support and investigated for ammonia cracking at 400 °C. Previous studies suggest that single-atom catalysts, in the absence of strong metal-support interactions, exhibit ineffective ammonia decomposition. However, Ru/MgO(111) with atomic Ru dispersion (below 3.1 wt% loading) shows superior catalytic performance. As shown in Fig. 13(a), the reaction rate follows a double-volcano trend, with neighbouring Ru atoms enhancing NH_3 decomposition efficiency through a synergistic effect. Furthermore, as shown in Fig. 13(c) and (d), Ru species on MgO(111) support remains atomically dispersed, forming single atoms and 2D raft-like structures without 3D aggregation or metallic lattice, even at higher coverage. Therefore, it can be concluded that the atomically dispersed Ru-based nanocatalyst exhibited an impressive hydrogen spillover effect in a specific environment, enhancing ammonia decomposition. These catalysts not only showed excellent low-temperature catalytic activity but also reduced the required Ru content.

DFT modelling studies were also performed on Ru/MgO catalyst[37] and they revealed a decrease in TOF as Ru loading increased from 0.1 wt% to 5 wt%, attributed to the transition from single atoms to nanoparticles (Fig. 14). This finding highlights the superior activity of isolated Ru atoms over Ru nanoparticles containing B5 sites, challenging the conventional view of higher activity in clustered forms. Ammonia decomposition progresses through a key intermediate step involving

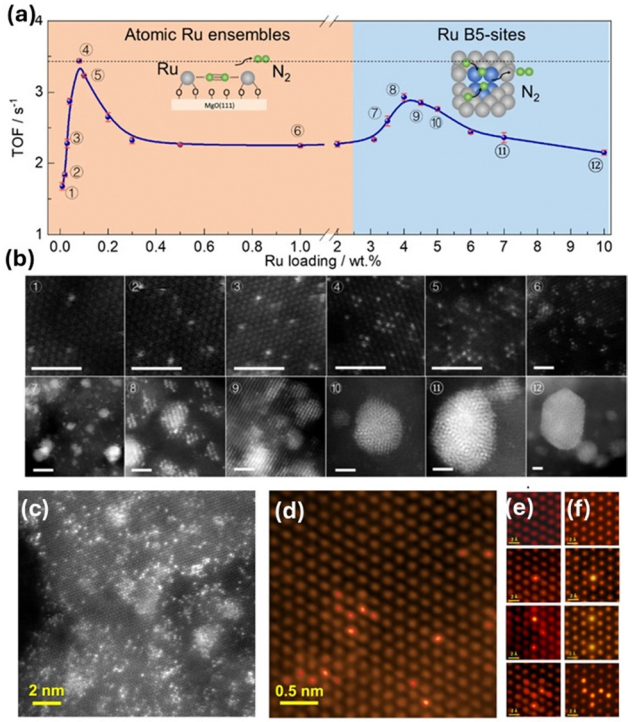

Fig. 13 (a) The TOF values with error bars for ammonia decomposition as a function of Ru loading at 400 °C; the error bars in the figure represent standard deviation through three repeated measurements; (b) typical STEM images of Ru/MgO(111) with different loadings, the labelled numbers are corresponding to the samples in a; the scale bar in white is 1 nm. (c) HAADF-STEM images of 3.1 wt% Ru/MgO(111), the scale bar in yellow is 2 nm; (d) HAADF-STEM images with observed single Ru atoms in the form of single Ru atoms, 2 × Ru atoms, 3 × Ru atoms and other close-by surface Ru atoms; the scale bar in yellow is 0.5 nm; (e) experimental image, and (f) image simulation. (Reproduced from ref. 37. Copyright (2023), with permission from Nature).

two Ru≡N surface species, which form a bimetallic nitrido-species complex with a μ-η^1:η^2 structure. This complex acts as an intermediate in homogeneous systems, facilitating the conversion of nitrogen atoms into N_2. The formation of this intermediate plays a crucial role in lowering the energy barrier for nitrogen recombination, ultimately enhancing the efficiency of ammonia decomposition.[37]

In another study, Teng *et al.*[46] synthesized that highly atomically dispersed Ru SACs on defective CeO_2 support and found that the presence of oxygen vacancies in CeO_2 supported single atom Ru catalysts exhibits an ammonia decomposition conversion of 91.2% at 450 °C under the condition of GHSV = 12 000 mL g_{cat}^{-1} h^{-1}. Furthermore, the hydrogen production rate per unit of Ru is as high as 2446 mmol g_{Ru}^{-1} min^{-1} with a TOF value of 8.09 s^{-1}. A microkinetic study was conducted on Ru, Ir, and Rh single-atom catalysts supported on graphene and nitrogen-modified graphene to explore the catalytic process of NH_3 cracking.[154] The results showed that nitrogen-modified graphene exhibited stronger interactions with metal atoms compared to vacancy graphene, offering enhanced resistance to metal sintering and leaching. This improved stability makes

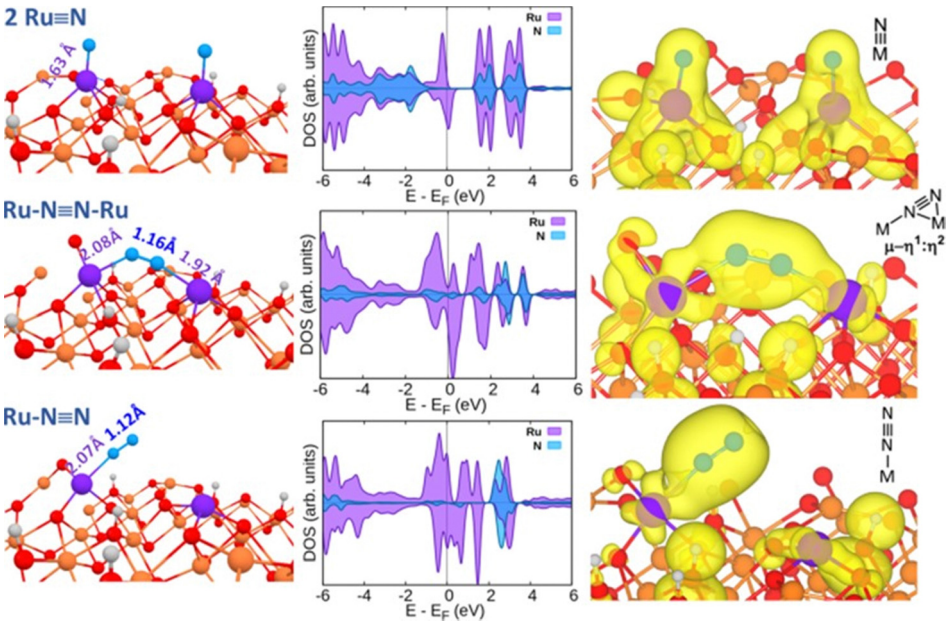

Fig. 14 Optimized structures, partial density of state and partial charge density of intermediate on Ru/MgO(111). (Reproduced from ref. 37. Copyright (2023), with permission from Nature).

nitrogen-modified graphene a more effective support for single-atom catalysts in ammonia decomposition.

Recently, Leung *et al.*[107] synthesized 13X zeolite-supported Ru single-atom catalysts (0.25 wt% loading) and exhibited the highest specific catalytic activity of over 4000 h^{-1} for the ammonia cracking at 450 °C. Numerous studies in the literature have detailed the homolytic cleavage of NH_3 into N_2 and H_2 over extended metal sites. However, isolated Ru sites, in combination with nearby H^+-depleted O sites from Brønsted acid sites (BAS), can activate NH_3 through a Frustrated Lewis Pair (FLP)-type mechanism. This synergistic interaction not only facilitates NH_3 activation but also regenerates the proton sites, as demonstrated by neutron powder diffraction (NPD) Rietveld refinement and supported by computational chemistry calculations, as illustrated in Fig. 15.

4.2. Metal cluster catalysts

Several researchers synthesized single-atom catalysts and transformed them into metal clusters under various conditions such as high temperature and reductive atmospheres such as hydrogen gas. Metal cluster catalysts have garnered significant attention in heterogeneous catalysis due to their distinctive properties, such as high efficiency of active species, strong metal-support interactions, and unsaturated coordination of active metal atoms. Both free-standing and supported metal clusters exhibit unique chemical and physical characteristics that change with size, as each cluster features a specific electron confinement profile. This size-dependent behavior allows for tailored catalytic performance, making metal clusters a highly promising avenue in catalyst design.

It was demonstrated that Ru clusters decorated on CeO_2 support catalysts exhibited superior catalytic performance over single metal and nanoparticles due to the balanced SMSI and H-spillover effects. However, the transformation of single atoms to uniform clusters can be restricted if there is no proper support and forms larger uncontrolled nanoparticles, which are drawbacks for ammonia cracking applications. Supported Ru nanoparticles, typically larger than 2 nm, have been widely employed in ammonia decomposition to produce high-purity hydrogen, which is essential for fueling proton exchange membrane fuel cells (PEMFCs). Their catalytic efficiency makes them an ideal choice for this application, enabling a clean and efficient hydrogen generation process for PEMFCs. These catalysts have shown superior activity compared to other materials studied for this reaction.[70] However, their practical use is restricted by the need for high Ru loading (>4 wt%) and operating temperatures exceeding 450 °C. Stabilized Ru clusters on suitable supports may offer a more viable alternative for broader applications.

Recently, Hu *et al.*[52] synthesized Ru single atoms with low loadings (0.3–1.0 wt%) on CeO_2 support with nanorods structure using a colloidal deposition approach (Fig. 16). Further, the as-prepared atomically dispersed Ru single atoms were converted to highly stable and uniform Ru clusters, approximately 1.5 nm in size under an ammonia atmosphere at 550 °C.

To enhance the atomic efficiency of catalysts, reducing noble metals to sub-nanometer clusters with 100% dispersion has been suggested as a simple and effective strategy. This approach maximizes exposure of catalytically active edge and corner sites, significantly boosting performance across various reactions.[155] From this perspective, Li *et al.*[112] downsized Ru nanoparticles to clusters (sub-nm < 1 nm) by using metal–organic framework such as MIL-101 as a host and investigated for ammonia decomposition. The study found that the catalytic

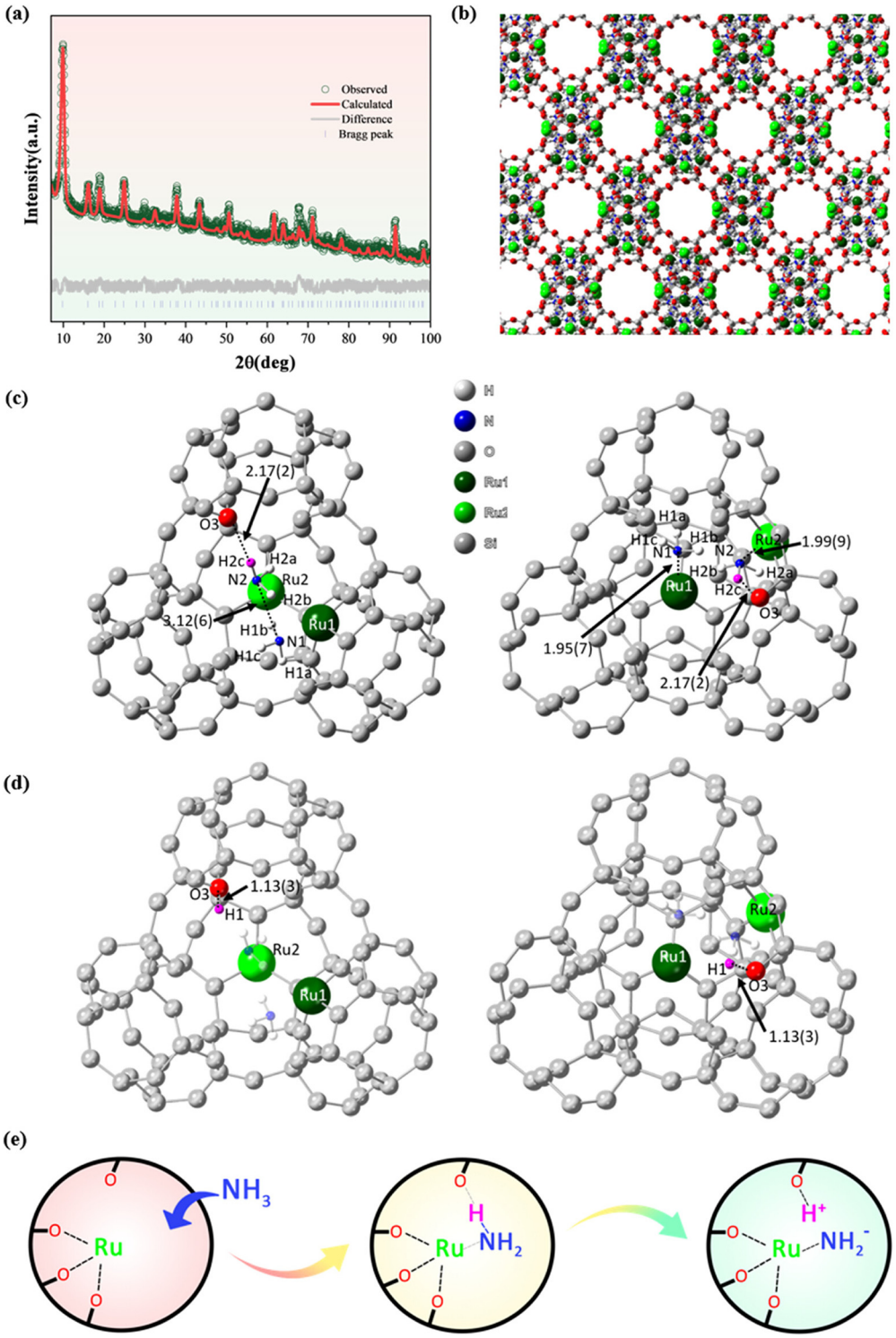

Fig. 15 (a) Original and Rietveld refinement fit of NPD data of X1.4H-RT (R_{wp} = 2.375%, R_{exp} = 1.865%, gof = 1.2736). (b) Zeolite structure showing the determined proton sites and NH_3 molecules of X1.4H-RT *via* NPD-Rietveld refinement. The atoms are labeled according to the element (dark green = Ru1, light green = Ru2, red = O, gray = Si and Al, blue = N and white = H). (c) Zeolite structure with the determined NH_3 molecules of X1.4H-RT with the bond length information (in Å) *via* NPD-Rietveld refinement. All O atoms are turned into gray color except the O atom (O3) that is located close to the proton H2c (in pink) of the adsorbed NH_3 of Ru2 and is able to undergo the FLP-type dissociation mechanism. (d) Zeolite structure containing regenerated proton sites on O atoms and NH_3 molecules of X1.4H-450 with given bond length information (in Å) *via* NPD-Rietveld refinement. All O atoms are turned into gray color except the O atom (O3) that undergoes the FLP-type dissociation mechanism and the corresponding proton H1 (in pink). (e) Proposed FLP-type mechanism for the N–H cleavage that occurred between NH_3 gas and the Ru sites in the Ru-loaded 13X zeolite. (Reproduced from ref. 107. Copyright (2023), with permission from ACS Publications).

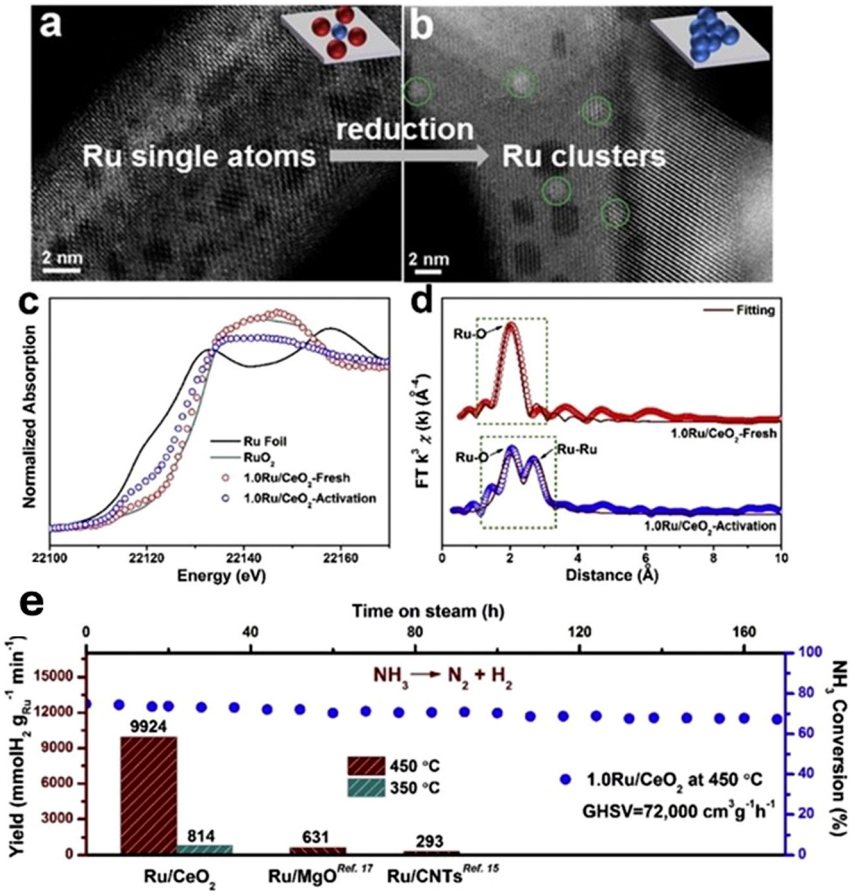

Fig. 16 The aberration-corrected HAADF-STEM images of the 1.0Ru/CeO_2 catalysts: (a) fresh; (b) after NH_3 activation. Green circles: typical Ru clusters. Schematic description of Ru single atoms and Ru clusters as inset. (c) *Ex situ* XANES profiles and (d) *ex situ* EXAFS spectra of the 1.0Ru/CeO_2 catalysts. (e) Comparison of H_2 formation yields (mmol H_2 g_{Ru}^{-1} min^{-1}) over 1.0Ru/CeO_2 catalyst and Ru/MgO, Ru/CNTs catalysts at 450 °C and 350 °C and the long-term stability of the 1.0Ru/CeO_2 catalyst tested for 168 h at 450 °C. (Reproduced from ref. 52. Copyright (2020), with permission from Elsevier).

activity of the Ru clusters is 500 times greater than that of the promoted Ru nanoparticle (NP) counterpart. Moreover, the catalyst demonstrated excellent stability, maintaining its activity for 40 hours without any increase in cluster size, highlighting its durability and resistance to sintering. Meng *et al.*[104] further improved the ammonia decomposition activity of Ru clusters supported on Al_2O_3 by incorporating CeO_2. In this study, a facile colloidal deposition method was used to load the Ru (0.5, 1, and 3 wt%) and found that very high hydrogen yield of 7097 mmol H_2 (g_{Ru}^{-1} min^{-1}) at 450 °C, which was described in Fig. 17. It is confirmed that Ru species are highly dispersed on the support surface as stable small clusters (~1.3 nm).

In another study, a 2D porous framework was utilized as a support to anchor Ru metal clusters, which effectively prevented cluster aggregation during ammonia decomposition. To investigate the effect of 2D support, the Ru clusters were prepared in two distinct polymer networked structures-vertically standing 2D structure (V2D), and planar 2D (P2D). This approach demonstrated an exceptional hydrogen production rate of 95.17 mmol g_{Ru}^{-1} min^{-1} at a high flow rate of 32 000 mL g_{cat}^{-1} h^{-1} at 450 °C.[106] As illustrated in Fig. 18, TEM images confirmed that the Ru nanoparticles in the Ru-V2D catalyst maintained their size and morphology post-reaction. In contrast, particle sizes increased significantly in the Ru-P2D and Ru/C catalysts after the catalytic reaction, indicating better stability for the Ru-V2D system. Ru-P2D particles grew from 5 to 10 nm, while Ru/C exhibited larger particles up to 50 nm. The V2D structure effectively blocked aggregation through vertical carbon obstructions, ensuring stable long-term activity during ammonia decomposition. Leung *et al.*[107] used crystalline and nanoporous aluminosilicate materials like zeolites as anchored supports to disperse the Ru metal clusters and investigated for ammonia decomposition. The authors performed DFT studies and found that nitrogen substitution in MFI zeolite improved higher dispersion of Ru species as anchored clusters, which improved NH_3 decomposition.

4.3. Support and additive effects on single atom and metal cluster catalysts

Support materials play a pivotal role in influencing the performance of catalysts in ammonia cracking. Supports affect the dispersion, electronic structure, and stability of metal clusters, or single atoms, thus impacting their catalytic activity. It was

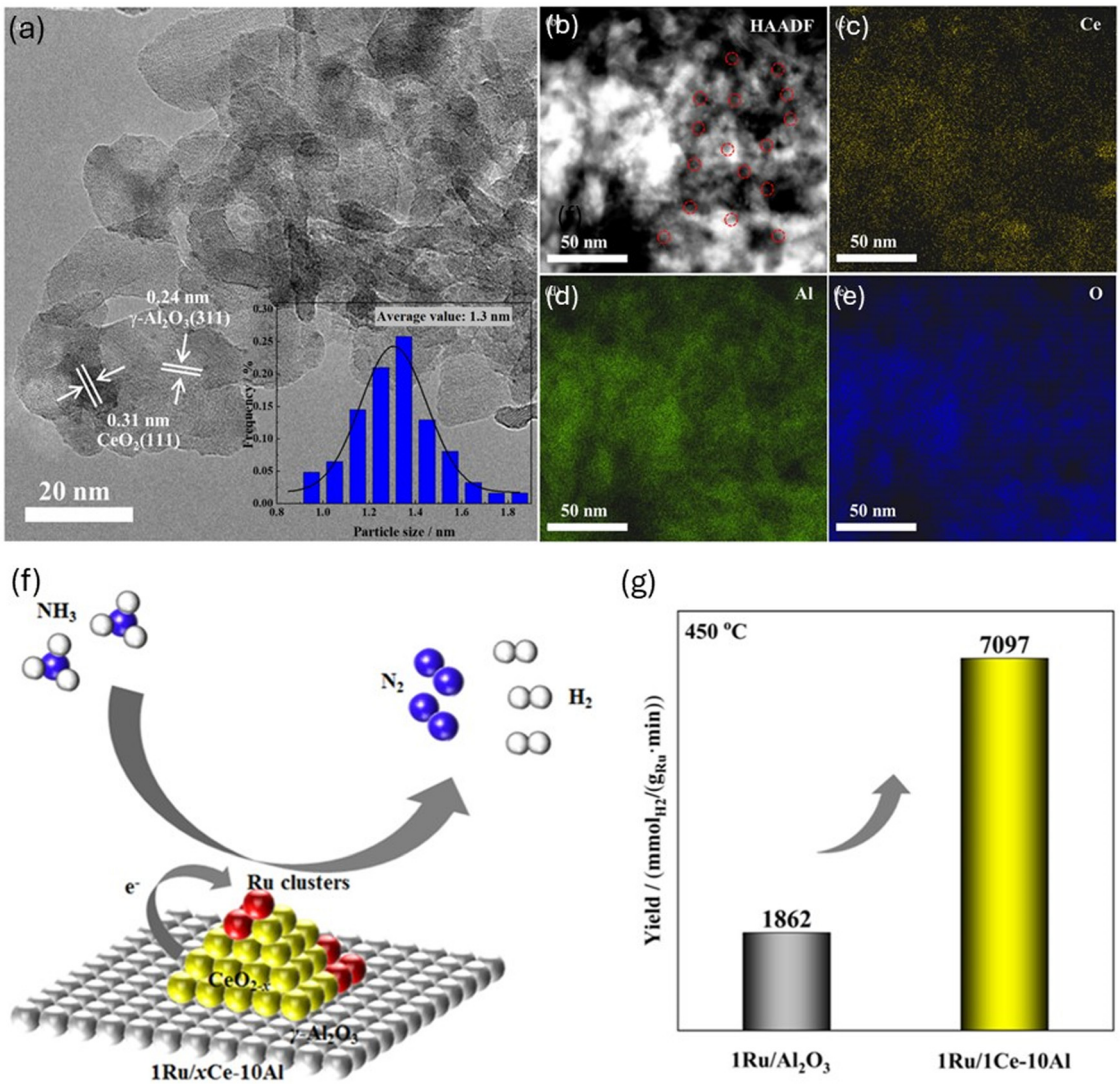

Fig. 17 (a) HRTEM image and particle size distribution (inset); (b) HAADF image (the Ru clusters are marked with red circles); (c)–(e) EDS elemental mapping images including Ce, Al, and O of used 1Ru/1Ce–10Al catalyst. (f) Graphical representations of Ru clusters are dispersed on Ce–Al support and enhanced hydrogen yield. (Reproduced from ref. 104. Copyright (2023), with permission from Elsevier).

discussed in various reviews that the interaction between metal species and support materials determines charge transfer characteristics, binding energies, and active site availability.[156] For instance, CeO_2, Al_2O_3, MgO, zeolites and carbon-based supports like graphene enhance catalytic efficiency by modifying the electronic environment of the metal centers. The synergy between metal and support facilitates optimal hydrogen adsorption and desorption dynamics during ammonia decomposition. Recent advances highlighted in the work by Hu *et al.*[52] emphasize that Ru single-atom catalysts exhibit unique interactions with CeO_2 support due to their isolated atomic sites. Compared to MgO and CNTs, CeO_2 support favoured the formation of stable Ru clusters with a size of 1.5 nm and the Ru/CeO_2 catalyst exhibited an outstanding H_2 yield of 9.924 mmol H_2 g_{Ru}^{-1}, which is approx. 15 and 34 times more than that of MgO and CNTs supports, respectively. This results in improved atom utilization and active site uniformity compared to traditional nanoparticles. Supports engineered with functional groups or defects enable strong metal-support interactions, enhancing catalyst stability and activity under reaction conditions.

Additionally, synthesis methods significantly influence the activity and stability of cluster and single-atom catalysts. Liu and Corma[157] emphasize the importance of precise synthetic strategies, such as atomic layer deposition (ALD) and wet chemical methods, to achieve uniform dispersion and strong metal-support interactions. Peng *et al.*[158] suggests that defect engineering in supports, combined with controlled precursor decomposition, is critical for anchoring single atoms. For instance, materials like zeolites and similar porous supports are often employed to achieve a narrower size distribution in catalysts.[159] These supports, with their abundant channels and cavities, effectively confine metal clusters and provide anchoring sites for active metals. However, despite these advantages,

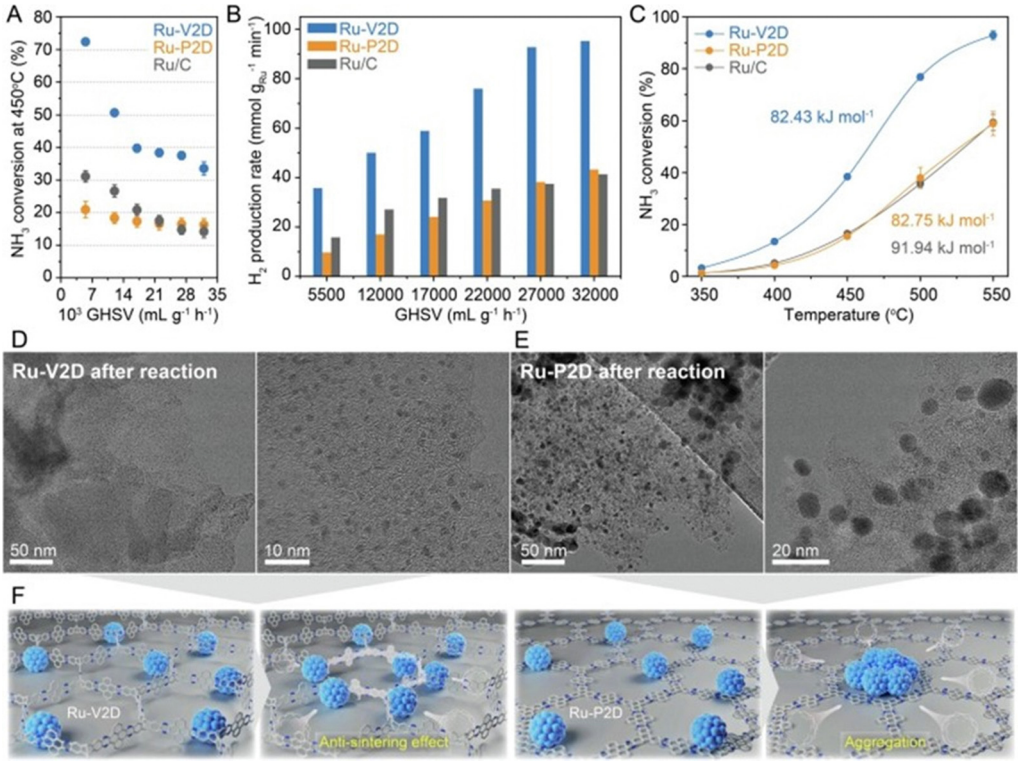

Fig. 18 Ammonia decomposition study under practical gas flow and reaction temperatures. (A) Ammonia decomposition conversion graph at 450 °C according to flow rates. (B) Hydrogen production rate per Ru contents (mmol g_{Ru}^{-1} h^{-1}) at 450 °C in each structure. (C) Decomposition conversion curves and activation energy of each structure at P = 1 atm; T = 350–550 °C, GHSV: 22 000 mL g_{cat}^{-1} h^{-1}. (D) and (E) TEM images of Ru-V2D (D) and Ru-P2D (E) after ammonia decomposition reaction. (F) Illustration of the anti-sintering effect of the V2D *vs.* P2D structure. (Reproduced from ref. 106. Copyright (2023), with permission from Elsevier).

zeolite-supported metal clusters frequently experience coalescence under reactive gas flow conditions. This challenge arises due to insufficient metal-support interactions and the limited capacity of the porous channels to stabilize the cluster. Recently, Li *et al.*[159] used a host–guest strategy based on a metal-linked porous materials, in which MIL-101 MOFs were used to synthesize Ru clusters on MgO support and investigated for NH_3 decomposition. As shown in Fig. 19(a), sub-nm Ru clusters were dispersed on MgO support using the sacrificed template (MIL-101). This synthesis method offered smaller Ru clusters ($<$1 nm) compared to traditional precipitation method ($>$1 nm). Further, the additives such as Cs promoted the ammonia conversion of Ru/MgO-MIL catalyst and highest activity observed over Ru/AC, which indicates that the verifying the effect of the support and promoter as well as the metal–support interactions between Ru and the promoters.

Together, these insights provide a comprehensive understanding of the interplay between support effects, synthesis techniques, and the performance of single-atom and cluster catalysts in ammonia cracking, paving the way for further advancements in sustainable hydrogen production.

5. Microkinetic modelling studies

Microkinetic modelling provides a detailed mechanistic understanding of the ammonia decomposition reaction, a critical process for hydrogen production. Ammonia decomposition follows a Langmuir–Hinshelwood mechanism[160] and this reaction, $2NH_3 \rightleftharpoons N_2 + 3H_2$ involves multiple elementary steps: ammonia adsorption, N–H bond scission, nitrogen recombination, and desorption of products (N_2 and H_2).[161,162] The rate-determining step (RDS) is often identified as the nitrogen recombination or the scission of the N–H bond, depending on the catalyst.[163] Various metals such as Ru, Fe, Co, Ni, and their alloys are extensively studied and among them, Ru-based catalysts are highly active due to their optimal binding energies for reaction intermediates.

Most of the published research works on ammonia decomposition revealed the kinetic studies of this reaction using first principal calculations or density functional theory (DFT) studies. These studies highlight the significance of integrating experimental and computational approaches, such as DFT calculations and microkinetic modelling, to understand and optimize catalysts for ammonia decomposition. For example, Gascon and co-workers[164] reported that Ru-based catalysts, such as Ru/CaO and Ru–K/CaO, demonstrate superior activity, with potassium (K) promotion significantly altering surface properties, enhancing N_2 desorption, and shifting the rate-determining step (RDS). Alternative catalysts, such as Ba-promoted Co–Ce systems prepared by Gontzal *et al.*,[165] offer promising performance at higher temperatures, with Ba improving nanoparticle dispersion and exposing more active

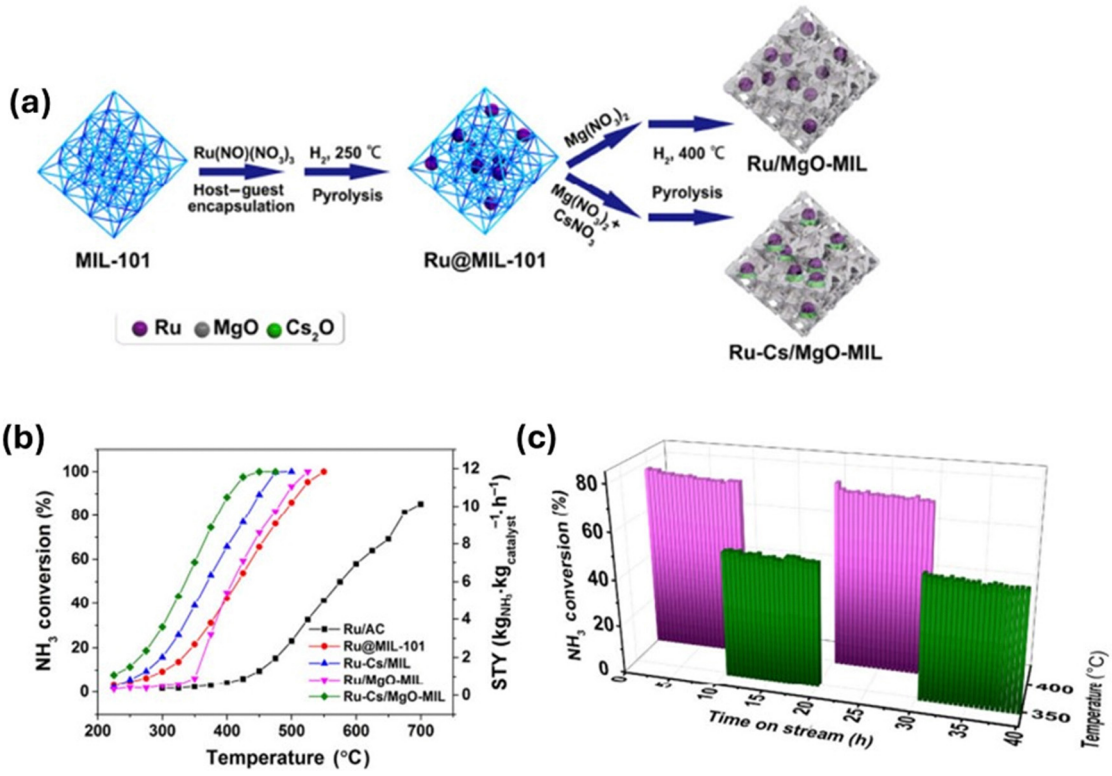

Fig. 19 (a) Schematic synthetic protocols of MIL-101-confined Ru clusters, (b) NH_3 conversion (left column) and the corresponding STY values (right column) for ammonia decomposition catalyzed by MOF-encapsulated Ru clusters and references. (c) Stability test of ammonia decomposition catalyzed by promoted Ru cluster. Reaction condition: 100 mg of catalysts, 25 mL min^{-1} of NH_3 flow rate, 1 bar. (Reproduced from ref. 112. Copyright (2018), with permission from Springer Nature).

sites, thereby accelerating key steps like N_2 desorption and NH_2 dehydrogenation. It was found from *ab initio* calculations and discovered that two different rate determining steps for the Ru/CaO and Ru–K/CaO catalysts.[166] Fig. 20 shows the potential surface diagrams from the fitted models and clearly indicating that the addition of promoter altering the RDS at the microkinetic level. These findings challenge traditional models like the Temkin–Pyzhev approach by providing *ab initio* insights into catalytic behavior. The use of thermodynamically consistent microkinetic models reveals critical mechanistic details, underscoring the limitations of global rate expressions that rely on oversimplified assumptions. Collectively, these advancements provide a robust platform for developing next-generation ammonia-cracking catalysts, emphasizing the role of promoters, support effects, and comprehensive reaction modelling.

Similar to metal nanoparticles, there are few DFT studies were performed on single-atom catalysts. Recently, Xiuyuan and Alberto[154] investigated the NH_3 cracking reaction mechanism on single-atom catalysts (SACs) supported by

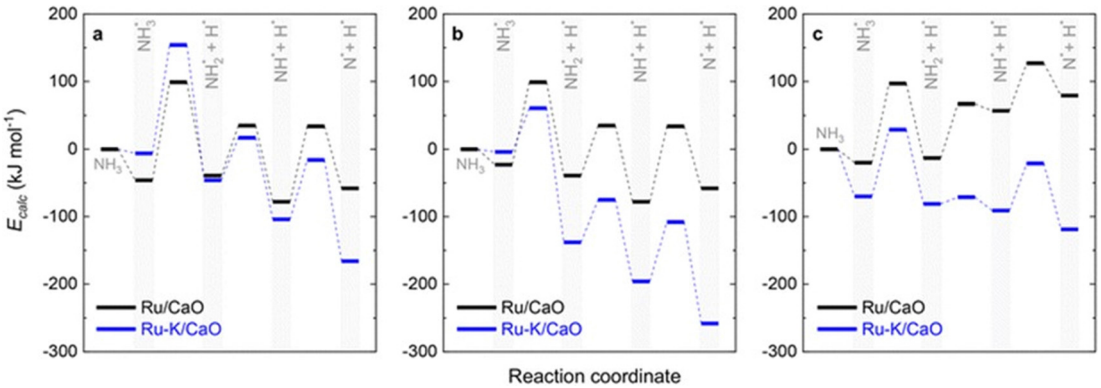

Fig. 20 Potential surface diagrams considering the obtained activation energies from the fitted models: (a) case A (NH_3 dissociation); (b) case B (N_2 desorption); and (c) case C (NH dissociation). (Reproduced with permission from ref. 166 from the Royal Society of Chemistry).

nitrogen-modified graphene revealed that the most favorable adsorption site is directly atop the metal atom. Relative energy calculations indicated that MN_3 structures exhibit higher activity than MN_4, as the MN_3 configuration promotes electron back-donation, thereby enhancing the activation of the N–H bond. The findings showed that, on SACs, the first dehydrogenation of NH_3 and the evolution of N_2 are the rate-determining steps in the reaction mechanism. Ir, Ru, and Rh emerged as the most promising candidates. Thermochemical analysis, with free energy calculations for molecular and adsorbed species between 200 and 1000 K, showed minimal temperature-based variations in reaction and activation energies.

In addition to noble metal, several researchers performed DFT calculations on non-noble metal clusters including Ni_6, Co_6, and Fe_6 supported by graphene ($Mx = Ni_6$, Co_6, Fe_6),[154] and focussed on the adsorption of NH_3, the NH_2–H bond cleavage, the N migration and N + N recombination to evaluate the catalytic activity. The Ni_6 cluster on graphene showed the highest activity for NH_3 adsorption, with an order of $Fe_6 < Co_6 < Ni_6$. For Ni_6 and Ni_6@graphene, the rate-limiting step is N + N recombination, with Ni_6@graphene reducing reaction barriers more effectively than the Ni_6 cluster alone.

6. Comparison of Ru SACs, metal clusters, and NPs

Table 2 consists of the information on the properties of Ru SACs, metal clusters, and NPs and their activity comparisons. For Ru/CeO_2, Ru clusters demonstrated the highest activity for hydrogen production from ammonia cracking, achieving 9924 mmol g_{Ru}^{-1} min^{-1}, whereas Ru nanoparticles on the same support exhibited only 22.5 mmol g_{Ru}^{-1} min^{-1}---indicating a 441-fold increase in activity. Similarly, for Ru/MgO, single atoms and clusters showed significantly higher activity (1857 mmol g_{Ru}^{-1} min^{-1}) compared to Ru nanoparticles (18.9 mmol g_{Ru}^{-1} min^{-1}). These results highlight the influence of synthesis methods and support effects, with CeO_2 exhibiting superior catalytic performance. The Ru loading ratio is a key factor in controlling Ru size, with low loadings (<1 wt%) being optimal for forming Ru single-atom/cluster species, thereby enhancing NH_3 decomposition efficiency.

7. Conclusions, challenges, and future directions

Ammonia cracking offers a promising pathway for efficient hydrogen production, leveraging the well-established infrastructure for ammonia synthesis and distribution. Noble metal catalysts, particularly ruthenium, have demonstrated exceptional performance in ammonia decomposition. However, addressing the research gaps related to catalyst cost, stability, support materials, reaction mechanisms, system integration, and safety considerations is crucial for advancing this technology. Continued research and development in these areas will pave the way for sustainable and economically viable hydrogen production from ammonia, contributing to the global transition towards a clean and low-carbon energy future.

The development of Ru-based catalysts for ammonia synthesis and decomposition has made significant strides, yet several challenges remain. The high cost of Ru, the need for precise control over catalyst synthesis, and the complexity of metal-support interactions continue to pose obstacles. Future research should focus on developing cost-effective synthesis methods that allow for precise control over Ru nanoparticle formation, exploring novel support materials, and gaining a deeper understanding of reaction mechanisms. The core challenge in designing effective Ru-based catalysts lies in accelerating the rate-determining steps of ammonia synthesis and decomposition. For ammonia synthesis, this primarily involves the activation of N_2, while in ammonia decomposition, it centres on weakening the Ru–N bond. Various strategies have been employed to address these challenges, including nanoscale engineering, the construction of composites, and the enhancement of support effects and promoter interactions.

Table 2 Comparison of catalytic efficiencies of previously reported Ru NP-, SACs-, and metal clusters-based catalysts for ammonia decomposition

Catalyst	Ru content (wt%)	Ru structure	Reaction conditions	Rate of H_2 formation (mmol g_{Ru}^{-1} min^{-1})	TOF_{H_2}[a] (s^{-1})	Ref.
Ru/CeO_2	1	Clusters	450 °C, GHSV = 228 000 NH_3 cm^3 g_{cat}^{-1} h^{-1}	9924	—	52
Ru/CeO_2	1	Clusters	350 °C, GHSV= 22 000 NH_3 cm^3 g_{cat}^{-1} h^{-1}	814	—	52
Ru/CeO_2	1	Clusters	340 °C, GHSV = 110 000 NH_3 cm^3 g_{cat}^{-1} h^{-1}	1618	3.2	52
Ru/CeO_2	1	NPs	450 °C, GHSV = 22 000 NH_3 cm^3 g_{cat}^{-1} h^{-1}	22.5	—	52
Ru/MgO	1	Single atoms Clusters	450 °C, GHSV = 36 000 NH_3 cm^3 g_{cat}^{-1} h^{-1}	1857	—	52
Ru/MgO	3.5	NPs	450 °C, GHSV = 36 000 NH_3 cm^3 g_{cat}^{-1} h^{-1}	998	—	51
Ru/MgO-DP	3.5	NPs	450 °C, GHSV = 30 000 NH_3 cm^3 g_{cat}^{-1} h^{-1}	18.9	3	82
Ru/Al_2O_3	1.1	Clusters	350 °C, GHSV = 22 000 NH_3 cm^3 g_{cat}^{-1} h^{-1}	83	0.2	52
Ru/Al_2O_3	4	NPs	450 °C, GHSV = 12 000 NH_3 cm^3 g_{cat}^{-1} h^{-1}	301	—	57
Ru/Al_2O_3	4.7	Clusters	500 °C, GHSV = 30 000 NH_3 cm^3 g_{cat}^{-1} h^{-1}	26.8	—	167
Ru/CNTs	5	NPs	450 °C, GHSV = 30 000 NH_3 cm^3 g_{cat}^{-1} h^{-1}	293	—	31
Ru/CNTs	5	NPs	350 °C, GHSV = 30 000 NH_3 cm^3 g_{cat}^{-1} h^{-1}	42	0.3	31
Ru CNT	4.8	NPs	450 °C, GHSV = 30 000 NH_3 cm^3 g_{cat}^{-1} h^{-1}	14.5	2.41	105
Ru/AC	4.8	NPs	450 °C, GHSV= 30 000 NH_3 cm^3 g_{cat}^{-1} h^{-1}	9.6	1.64	105
Ru/MgAl	2.09	Clusters	450 °C, GHSV= 30 000 NH_3 cm^3 g_{cat}^{-1} h^{-1}	12	2.05	168
Ru/Ce_5/MgAl	1.98	Clusters	450 °C, GHSV = 30 000 NH_3 cm^3 g_{cat}^{-1} h^{-1}	27.4	3.89	168

[a] TOF_{H_2}: turnover frequency values calculated based on H_2 formation yield at a low NH_3 conversion below 15%.

Nanoscale engineering has proven to be a powerful tool in optimizing the catalytic performance of Ru-based systems. By controlling the size and shape of Ru nanoparticles, researchers can maximize the number of active sites, such as the B5 sites, which are known to be the most efficient for ammonia synthesis. Despite significant progress, achieving uniform Ru-based catalysts with well-designed structures, high dispersion, and precise metal–support interfaces remain challenging. Traditional synthesis methods like impregnation, precipitation, and chemical reductions often fall short of providing the necessary control over nanoparticle formation. As a result, advanced techniques such as atomic layer deposition (ALD) and chemical vapour deposition (CVD) have gained attention. These methods allow for the bottom-up synthesis of supported metal catalysts, offering precise control over the size, composition, and structure of Ru nanoparticles.

Additionally, the potential of bimetallic and multimetallic catalysts, as well as the incorporation of promoters, offers exciting opportunities for further enhancing catalytic performance. The integration of advanced characterization techniques, both *in situ* and *ex situ*, will be essential for unravelling the complex interactions within these catalysts and guiding the design of next-generation systems. Despite the promising potential of noble metal catalysts for ammonia cracking, several research gaps need to be addressed to fully realize the benefits of this technology: noble metals are expensive and relatively scarce. Research is needed to develop cost-effective catalysts that either reduce the amount of noble metal required or use alternative materials that provide similar catalytic performance.[38] Long-term stability and resistance to deactivation are critical for the practical application of ammonia-cracking catalysts. Understanding the mechanisms of catalyst deactivation and developing strategies to enhance catalyst durability are essential areas of research. The choice of support material can significantly influence the activity, selectivity, and stability of noble metal catalysts. Research on novel support materials and their interactions with noble metals is crucial for optimizing catalyst performance. A deeper understanding of the fundamental reaction mechanisms and kinetics of ammonia cracking is needed to design more efficient catalysts.[34]

However, an exciting frontier in this field is the exploration of single atoms and metal clusters as catalysts for ammonia cracking. Single-atom catalysts (SACs) represent a transformative approach by maximizing the utilization of noble metals like Ru, as each atom acts as an active site. This not only reduces the overall metal usage but also enhances the catalytic efficiency by providing highly uniform and dispersed active sites. SACs, anchored on carefully designed support materials, have shown promise in breaking Ru–N bonds, which is the rate-determining step in ammonia decomposition. Metal clusters, consisting of a few atoms, further bridge the gap between single atoms and larger nanoparticles, offering high activity while maintaining relatively low metal content.

The shift towards SACs and metal clusters could propel ammonia cracking research to the next level by addressing the key limitations of traditional Ru-based catalysts. This advancement would not only reduce material costs but also open new possibilities for tuning catalyst properties, such as electronic structure and coordination environment, through atomic-level control. Furthermore, integrating advanced characterization techniques like *in situ* spectroscopy with computational modeling will be crucial to understand the intricate interactions at these smaller scales and guide the rational design of next-generation catalysts.

By harnessing the potential of SACs and metal clusters, future research can tackle the cost, stability, and reaction mechanism challenges, pushing ammonia cracking closer to commercial-scale hydrogen production. These advances contribute to the broader goal of establishing ammonia as a viable hydrogen carrier in the global shift towards cleaner, low-carbon energy solutions.

Data availability

No primary research results, software or code have been included, and no new data were generated or analysed as part of this review.

Conflicts of interest

There are no conflicts to declare.

Acknowledgements

This activity received funding from the Australian Renewable Energy Agency (ARENA) as part of ARENA's Hydrogen Research and Development Funding Round, awarded to Cavendish Renewable Technology Pty Ltd for the project titled Efficient, Scalable, and Modular Ammonia to Hydrogen/Electricity Conversion System (Grant number:GRT-RM-0200325229). The views expressed herein are not necessarily the views of the Australian Government, and the Australian Government does not accept responsibility for any information or advice contained herein.

References

1 I. Staffell, D. Scamman, A. Velazquez Abad, P. Balcombe, P. E. Dodds, P. Ekins, N. Shah and K. R. Ward, *Energy Environ. Sci.*, 2019, **12**, 463–491.
2 V. Balasubramanian, N. Haque, S. Bhargava, S. Madapusi and R. Parthasarathy, in *Bioenergy Resources and Technologies*, ed. A. K. Azad and M. M. K. Khan, Academic Press, 2021, pp. 195–218, DOI: 10.1016/B978-0-12-822525-7.00016-0.
3 P. Adamou, S. Bellomi, S. Hafeez, E. Harkou, S. M. Al-Salem, A. Villa, N. Dimitratos, G. Manos and A. Constantinou, *Catal. Today*, 2023, **423**, 114022.
4 S. S. Rathore, A. P. Kulkarni, D. Fini, S. Giddey and A. Seeber, *Solids*, 2021, **2**, 177–191.
5 Y. Wang, H. Arandiyan, S. S. Mofarah, X. Shen, S. A. Bartlett, P. Koshy, C. C. Sorrell, H. Sun, C. Pozo-Gonzalo, K. Dastafkan, S. Britto, S. K. Bhargava and C. Zhao, *Adv. Mater.*, 2024, **36**, 2402156.
6 V. Bansal, A. P. O'Mullane and S. K. Bhargava, *Electrochem. Commun.*, 2009, **11**, 1639–1642.

7 P. Saini, P. Koley, D. Damma, D. Jampaiah and S. K. Bhargava, *Chem. – Asian J.*, 2024, **19**, e202400752.
8 D. Jampaiah, D. Damma, P. Venkataswamy, A. Chalkidis, H. Arandiyan and B. M. Reddy, *Int. J. Hydrogen Energy*, 2023, **48**, 24860–24870.
9 L. Szablowski, M. Wojcik and O. Dybinski, *Energy*, 2025, **316**, 134540.
10 H. Arandiyan, S. S. Mofarah, Y. Wang, C. Cazorla, D. Jampaiah, M. Garbrecht, K. Wilson, A. F. Lee, C. Zhao and T. Maschmeyer, *Chem. – Eur. J.*, 2021, **27**, 14418–14426.
11 S. Manchala, V. S. R. K. Tandava, L. R. Nagappagari, S. M. Venkatakrishnan, D. Jampaiah, Y. M. Sabri, S. K. Bhargava and V. Shanker, *Photochem. Photobiol. Sci.*, 2019, **18**, 2952–2964.
12 D. Jampaiah, D. Shah, A. Chalkidis, P. Saini, R. Babarao, H. Arandiyan and S. K. Bhargava, *Langmuir*, 2024, **40**, 9732–9740.
13 R. Kumar, R. Singh and S. Dutta, *Energy Fuels*, 2024, **38**, 2601–2629.
14 S. Ristig, M. Poschmann, J. Folke, O. Gómez-Cápiro, Z. Chen, N. Sanchez-Bastardo, R. Schlögl, S. Heumann and H. Ruland, *Chem. Ing. Tech.*, 2022, **94**, 1413–1425.
15 S. Giddey, S. P. S. Badwal, C. Munnings and M. Dolan, *ACS Sustainable Chem. Eng.*, 2017, **5**, 10231–10239.
16 S. S. Rathore, S. Biswas, D. Fini, A. P. Kulkarni and S. Giddey, *Int. J. Hydrogen Energy*, 2021, **46**, 35365–35384.
17 J. Ashcroft and H. Goddin, *Johnson Matthey Technol. Rev.*, 2022, **66**, 375–385.
18 K. Trangwachirachai, K. Rouwenhorst, L. Lefferts and J. A. Faria Albanese, *Curr. Opin. Green Sustainable Chem.*, 2024, **49**, 100945.
19 L. Zhai, S. Liu and Z. Xiang, *Ind. Chem. Mater.*, 2023, **1**, 332–342.
20 D. Lim, J. A. Moon, Y. J. Koh, A. Zare Ghadi, A. Lee and H. Lim, *Chem. Eng. J.*, 2023, **468**, 143492.
21 K. Yamazaki, M. Matsumoto, M. Ishikawa and A. Sato, *Appl. Catal., B*, 2023, **325**, 122352.
22 M. Yue, H. Lambert, E. Pahon, R. Roche, S. Jemei and D. Hissel, *Renewable Sustainable Energy Rev.*, 2021, **146**, 111180.
23 X. Li, Q. Wang, S. Wu, Z. Hu and J. Bai, *Sustainable Chem. Pharm.*, 2024, **38**, 101492.
24 J. Zhang, L. Zheng, Y. Ma, Z. Cai, Y. Cao, K. Huang and L. Jiang, *Energy Fuels*, 2022, **36**, 14516–14533.
25 D. B. Akolekar, A. R. Hind and S. K. Bhargava, *J. Colloid Interface Sci.*, 1998, **199**, 92–98.
26 V. D. B. C. Dasireddy and B. Likozar, *Fuel*, 2017, **196**, 325–335.
27 Š. Hajduk, V. D. B. C. Dasireddy, B. Likozar, G. Dražić and Z. C. Orel, *Appl. Catal., B*, 2017, **211**, 57–67.
28 Y. Zhao, B. P. Setzler, J. Wang, J. Nash, T. Wang, B. Xu and Y. Yan, *Joule*, 2019, **3**, 2472–2484.
29 K. Omata, K. Sato, K. Nagaoka, H. Yukawa, Y. Matsumoto and T. Nambu, *Int. J. Hydrogen Energy*, 2022, **47**, 8372–8381.
30 Z. Zhao, M. Zhang, Y. Wu, W. Song, J. Yan, X. Qi, J. Yang, J. Wen and H. Zhang, *Ind. Eng. Chem. Res.*, 2024, **63**, 8003–8024.
31 S.-F. Yin, Q.-H. Zhang, B.-Q. Xu, W.-X. Zhu, C.-F. Ng and C.-T. Au, *J. Catal.*, 2004, **224**, 384–396.
32 C. Chen, K. Wu, H. Ren, C. Zhou, Y. Luo, L. Lin, C. Au and L. Jiang, *Energy Fuels*, 2021, **35**, 11693–11706.
33 E. Spatolisano, L. A. Pellegrini, A. R. de Angelis, S. Cattaneo and E. Roccaro, *Ind. Eng. Chem. Res.*, 2023, **62**, 10813–10827.
34 S. Sun, Q. Jiang, D. Zhao, T. Cao, H. Sha, C. Zhang, H. Song and Z. Da, *Renewable Sustainable Energy Rev.*, 2022, **169**, 112918.
35 H. A. Yousefi Rizi and D. Shin, *Energies*, 2022, **15**, 8246.
36 C. Zheng, B. Guan, J. Guo, T. Su, J. Zhou, J. Chen, Y. Zhang, Y. Yuan, W. Xie, N. Zhou and Z. Huang, *Ind. Eng. Chem. Res.*, 2023, **62**, 11305–11336.
37 H. Fang, S. Wu, T. Ayvali, J. Zheng, J. Fellowes, P.-L. Ho, K. C. Leung, A. Large, G. Held, R. Kato, K. Suenaga, Y. I. A. Reyes, H. V. Thang, H.-Y. T. Chen and S. C. E. Tsang, *Nat. Commun.*, 2023, **14**, 647.
38 Z. Su, J. Guan, Y. Liu, D. Shi, Q. Wu, K. Chen, Y. Zhang and H. Li, *Int. J. Hydrogen Energy*, 2024, **51**, 1019–1043.
39 T. Su, B. Guan, J. Zhou, C. Zheng, J. Guo, J. Chen, Y. Zhang, Y. Yuan, W. Xie, N. Zhou, H. Dang, B. Xu and Z. Huang, *Energy Fuels*, 2023, **37**, 8099–8127.
40 J. Nisar, S. Giddey, G. Kaur, A. P. Kulkarni, S. Biswas, L. A. Jones and S. K. Bhargava, *Ionics*, 2024, **30**, 5481–5494.
41 S. J. Wang, S. F. Yin, L. Li, B. Q. Xu, C. F. Ng and C. T. Au, *Appl. Catal., B*, 2004, **52**, 287–299.
42 A. K. Hill and L. Torrente-Murciano, *Appl. Catal., B*, 2015, **172–173**, 129–135.
43 S. F. Yin, B. Q. Xu, X. P. Zhou and C. T. Au, *Appl. Catal., A*, 2004, **277**, 1–9.
44 J. C. Ganley, F. S. Thomas, E. G. Seebauer and R. I. Masel, *Catal. Lett.*, 2004, **96**, 117–122.
45 T. V. Choudhary, C. Sivadinarayana and D. W. Goodman, *Catal. Lett.*, 2001, **72**, 197–201.
46 B. Teng, C. Ma, J. Chen, Y. Zhang, B. Wei, M. Sang, H. Wang and Y. Sun, *ACS Appl. Nano Mater.*, 2024, **7**, 15012–15024.
47 H. Fang, D. Liu, Y. Luo, Y. Zhou, S. Liang, X. Wang, B. Lin and L. Jiang, *ACS Catal.*, 2022, **12**, 3938–3954.
48 S. Mukherjee, S. V. Devaguptapu, A. Sviripa, C. R. F. Lund and G. Wu, *Appl. Catal., B*, 2018, **226**, 162–181.
49 O. A. Ojelade and S. F. Zaman, *Chem. Pap.*, 2021, **75**, 57–65.
50 F. Chang, W. Gao, J. Guo and P. Chen, *Adv. Mater.*, 2021, **33**, 2005721.
51 X. Ju, L. Liu, P. Yu, J. Guo, X. Zhang, T. He, G. Wu and P. Chen, *Appl. Catal., B*, 2017, **211**, 167–175.
52 X.-C. Hu, X.-P. Fu, W.-W. Wang, X. Wang, K. Wu, R. Si, C. Ma, C.-J. Jia and C.-H. Yan, *Appl. Catal., B*, 2020, **268**, 118424.
53 H. Liu, R. Zhang, S. Liu and G. Liu, *ACS Catal.*, 2024, **14**, 9927–9939.
54 K. Ogasawara, T. Nakao, K. Kishida, T.-N. Ye, Y. Lu, H. Abe, Y. Niwa, M. Sasase, M. Kitano and H. Hosono, *ACS Catal.*, 2021, **11**, 11005–11015.
55 J. Feng, L. Liu, X. Ju, J. Wang, X. Zhang, T. He and P. Chen, *ChemCatChem*, 2021, **13**, 1552–1558.
56 Z. Wang, Z. Cai and Z. Wei, *ACS Sustainable Chem. Eng.*, 2019, **7**, 8226–8235.
57 A. M. Karim, V. Prasad, G. Mpourmpakis, W. W. Lonergan, A. I. Frenkel, J. G. Chen and D. G. Vlachos, *J. Am. Chem. Soc.*, 2009, **131**, 12230–12239.
58 H. Tabassum, S. Mukherjee, J. Chen, D. Holiharimanana, S. Karakalos, X. Yang, S. Hwang, T. Zhang, B. Lu, M. Chen, Z. Tang, E. A. Kyriakidou, Q. Ge and G. Wu, *Energy Environ. Sci.*, 2022, **15**, 4190–4200.
59 K. Kishida, M. Kitano, Y. Inoue, M. Sasase, T. Nakao, T. Tada, H. Abe, Y. Niwa, T. Yokoyama, M. Hara and H. Hosono, *Chem. – Eur. J.*, 2018, **24**, 7976–7984.
60 L. Yao, T. Shi, Y. Li, J. Zhao, W. Ji and C.-T. Au, *Catal. Today*, 2011, **164**, 112–118.
61 L. Li, Y. Wang, Z. P. Xu and Z. Zhu, *Appl. Catal., A*, 2013, **467**, 246–252.
62 Z. Hu, J. Mahin, S. Datta, T. E. Bell and L. Torrente-Murciano, *Top. Catal.*, 2019, **62**, 1169–1177.
63 W. Zheng, J. Zhang, Q. Ge, H. Xu and W. Li, *Appl. Catal., B*, 2008, **80**, 98–105.
64 Y. Yu, Y.-M. Gan, C. Huang, Z.-H. Lu, X. Wang, R. Zhang and G. Feng, *Int. J. Hydrogen Energy*, 2020, **45**, 16528–16539.
65 C. Huang, Y. Yu, J. Yang, Y. Yan, D. Wang, F. Hu, X. Wang, R. Zhang and G. Feng, *Appl. Surf. Sci.*, 2019, **476**, 928–936.
66 K. Okura, T. Okanishi, H. Muroyama, T. Matsui and K. Eguchi, *ChemCatChem*, 2016, **8**, 2988–2995.
67 J. Zhang, H. Xu, X. Jin, Q. Ge and W. Li, *Appl. Catal., A*, 2005, **290**, 87–96.
68 X. Ju, L. Liu, X. Zhang, J. Feng, T. He and P. Chen, *ChemCatChem*, 2019, **11**, 4161–4170.
69 Z. Wang, Y. Qu, X. Shen and Z. Cai, *Int. J. Hydrogen Energy*, 2019, **44**, 7300–7307.
70 X.-Y. Guo, J.-H. Wang, Q. Zhang, T.-Z. Li, H. Dong, C.-J. Jia, C. Li and Y.-W. Zhang, *Appl. Catal., B*, 2024, **348**, 123844.
71 J. W. Makepeace, T. J. Wood, H. M. A. Hunter, M. O. Jones and W. I. F. David, *Chem. Sci.*, 2015, **6**, 3805–3815.
72 Y.-Q. Gu, Z. Jin, H. Zhang, R.-J. Xu, M.-J. Zheng, Y.-M. Guo, Q.-S. Song and C.-J. Jia, *J. Mater. Chem. A*, 2015, **3**, 17172–17180.
73 H. Liu, H. Wang, J. Shen, Y. Sun and Z. Liu, *Appl. Catal., A*, 2008, **337**, 138–147.
74 L. H. Yao, Y. X. Li, J. Zhao, W. J. Ji and C. T. Au, *Catal. Today*, 2010, **158**, 401–408.
75 L. Huo, B. Liu, H. Li, B. Cao, X.-C. Hu, X.-P. Fu, C. Jia and J. Zhang, *Appl. Catal., B*, 2019, **253**, 121–130.
76 Z.-W. Wu, X. Li, Y.-H. Qin, L. Deng, C.-W. Wang and X. Jiang, *Int. J. Hydrogen Energy*, 2020, **45**, 15263–15269.

77 C. Huang, H. Li, J. Yang, C. Wang, F. Hu, X. Wang, Z.-H. Lu, G. Feng and R. Zhang, *Appl. Surf. Sci.*, 2019, **478**, 708–716.
78 X.-K. Li, W.-J. Ji, J. Zhao, S.-J. Wang and C.-T. Au, *J. Catal.*, 2005, **236**, 181–189.
79 J. Ji, X. Duan, G. Qian, X. Zhou, G. Tong and W. Yuan, *Int. J. Hydrogen Energy*, 2014, **39**, 12490–12498.
80 P. Yu, J. Guo, L. Liu, P. Wang, G. Wu, F. Chang and P. Chen, *ChemSusChem*, 2016, **9**, 364–369.
81 H. Zhang, Y. A. Alhamed, Y. Kojima, A. A. Al-Zahrani, H. Miyaoka and L. A. Petrov, *Int. J. Hydrogen Energy*, 2014, **39**, 277–287.
82 P. Yu, J. Guo, L. Liu, P. Wang, F. Chang, H. Wang, X. Ju and P. Chen, *J. Phys. Chem. C*, 2016, **120**, 2822–2828.
83 G. Li, H. Nagasawa, M. Kanezashi, T. Yoshioka and T. Tsuru, *J. Mater. Chem. A*, 2014, **2**, 9185–9192.
84 S.-F. Yin, B.-Q. Xu, S.-J. Wang and C.-T. Au, *Appl. Catal., A*, 2006, **301**, 202–210.
85 J. Guo, Z. Chen, A. Wu, F. Chang, P. Wang, D. Hu, G. Wu, Z. Xiong, P. Yu and P. Chen, *Chem. Commun.*, 2015, **51**, 15161–15164.
86 J. Zhang, H. Xu, Q. Ge and W. Li, *Catal. Commun.*, 2006, **7**, 148–152.
87 S.-F. Yin, B.-Q. Xu, C.-F. Ng and C.-T. Au, *Appl. Catal., B*, 2004, **48**, 237–241.
88 Z. Kong, S. Liu, H. Liu and G. Liu, *Energy Fuels*, 2024, **38**, 6538–6546.
89 H. J. Lee and E. D. Park, *Catalysts*, 2022, **12**, 1203.
90 F. Zhiqiang, W. Ziqing, L. Dexing, L. Jianxin, Y. Lingzhi, W. Qin and W. Zhong, *Fuel*, 2022, **326**, 125094.
91 E. H. Cho, N. Jeon, B. S. Yoon, S. Kim, Y. Yun and C. H. Ko, *Appl. Surf. Sci.*, 2023, **608**, 155244.
92 K. S. Al-Thubaiti and Z. Khan, *Int. J. Hydrogen Energy*, 2020, **45**, 13960–13974.
93 T.-B. Chen, H. Rabiee, P. Yan, Z. Zhu and L. Ge, *Energy Fuels*, 2024, **38**, 5449–5456.
94 T. H. Ulucan, J. Wang, E. Onur, S. Chen, M. Behrens and C. Weidenthaler, *ACS Catal.*, 2024, **14**, 2828–2841.
95 M. Zhao, J. Wang, X. Wang, J. Xu, L. Liu, W. Yang, J. Feng, S. Song and H. Zhang, *Small*, 2023, **19**, 2205313.
96 X. Duan, G. Qian, X. Zhou, Z. Sui, D. Chen and W. Yuan, *Appl. Catal., B*, 2011, **101**, 189–196.
97 C. Huang, Y. Yu, X. Tang, Z. Liu, J. Zhang, C. Ye, Y. Ye and R. Zhang, *Appl. Surf. Sci.*, 2020, **532**, 147335.
98 W. Zhang, W. Zhou, Y. Li, J. Ren and Z. Wang, *Appl. Catal., B*, 2023, **330**, 122644.
99 D. Varisli and T. Rona, *CO_x* Free Hydrogen Production From Ammonia Decomposition Over Platinum Based Siliceous Materials, De Gruyter, 2012, vol. 10.
100 R. Antunes, R. Steiner, L. Marot and E. Meyer, *Int. J. Hydrogen Energy*, 2022, **47**, 14130–14140.
101 A. Di Carlo, L. Vecchione and Z. Del Prete, *Int. J. Hydrogen Energy*, 2014, **39**, 808–814.
102 Y. Li, L. Yao, Y. Song, S. Liu, J. Zhao, W. Ji and C.-T. Au, *Chem. Commun.*, 2010, **46**, 5298–5300.
103 I. Lucentini, A. Casanovas and J. Llorca, *Int. J. Hydrogen Energy*, 2019, **44**, 12693–12707.
104 Q. Meng, H. Liu, K. Xu, W. Wang and C. Jia, *J. Rare Earths*, 2023, **41**, 801–809.
105 S. F. Yin, B. Q. Xu, W. X. Zhu, C. F. Ng, X. P. Zhou and C. T. Au, *Catal. Today*, 2004, **93–95**, 27–38.
106 S.-J. Kim, T. S. Nguyen, J. Mahmood and C. T. Yavuz, *Chem. Eng. J.*, 2023, **463**, 142474.
107 K. C. Leung, S. Hong, G. Li, Y. Xing, B. K. Y. Ng, P.-L. Ho, D. Ye, P. Zhao, E. Tan, O. Safonova, T.-S. Wu, M. M.-J. Li, G. Mpourmpakis and S. C. E. Tsang, *J. Am. Chem. Soc.*, 2023, **145**, 14548–14561.
108 F. Wang, L.-d Deng, Z.-w Wu, K. Ji, Q. Chen and X.-m Jiang, *Int. J. Hydrogen Energy*, 2021, **46**, 20815–20824.
109 K. E. Lamb, M. D. Dolan and D. F. Kennedy, *Int. J. Hydrogen Energy*, 2019, **44**, 3580–3593.
110 L. Wang, J. Chen, L. Ge, V. Rudolph and Z. Zhu, *RSC Adv.*, 2013, **3**, 12641–12647.
111 J. M. G. Carballo, J. Yang, A. Holmen, S. García-Rodríguez, S. Rojas, M. Ojeda and J. L. G. Fierro, *J. Catal.*, 2011, **284**, 102–108.
112 J. Li, W. Wang, W. Chen, Q. Gong, J. Luo, R. Lin, H. Xin, H. Zhang, D. Wang, Q. Peng, W. Zhu, C. Chen and Y. Li, *Nano Res.*, 2018, **11**, 4774–4785.
113 C. J. H. Jacobsen, S. Dahl, P. L. Hansen, E. Törnqvist, L. Jensen, H. Topsøe, D. V. Prip, P. B. Møenshaug and I. Chorkendorff, *J. Mol. Catal. A: Chem.*, 2000, **163**, 19–26.
114 J. Gavnholt and J. Schiøtz, *Phys. Rev. B: Condens. Matter Mater. Phys.*, 2008, **77**, 035404.
115 F. R. García-García, A. Guerrero-Ruiz and I. Rodríguez-Ramos, *Top. Catal.*, 2009, **52**, 758–764.
116 N. Jeon, S. Kim, A. Tayal, J. Oh, W. Yoon, W. B. Kim and Y. Yun, *ACS Sustainable Chem. Eng.*, 2022, **10**, 15564–15573.
117 F. Qi, J. Peng, Z. Liang, J. Guo, J. Liu, T. Fang and H. Mao, *Environ. Sci. Ecotechnology*, 2024, **22**, 100443.
118 Y. Zhang, W. Yan, H. Qi, X. Su, Y. Su, X. Liu, L. Li, X. Yang, Y. Huang and T. Zhang, *ACS Catal.*, 2022, **12**, 1697–1705.
119 Y. Sun, G. Chen, S. Xi and Z. J. Xu, *ACS Catal.*, 2021, **11**, 13947–13954.
120 Y. Wang, J. Li and Z. Wei, *J. Mater. Chem. A*, 2018, **6**, 8194–8209.
121 S. Sahoo, K. Y. Wickramathilaka, E. Njeri, D. Silva and S. L. Suib, *Front. Chem.*, 2024, **12**, 1374878.
122 H. Yorimitsu, M. Kotora and N. T. Patil, *Chem. Rec.*, 2021, **21**, 3335–3337.
123 A. Mahsud, M. Arif, W. U. Khan, T. Zhang, S. Hussain, M. Azam and Z. Lu, *Mol. Catal.*, 2023, **550**, 113526.
124 I. Lucentini, G. García Colli, C. D. Luzi, I. Serrano, O. M. Martínez and J. Llorca, *Appl. Catal., B*, 2021, **286**, 119896.
125 I. Lucentini, I. Serrano, L. Soler, N. J. Divins and J. Llorca, *Appl. Catal., A*, 2020, **591**, 117382.
126 V. D. B. C. Dasireddy, Š. Hajduk, F. Ruiz-Zepeda, J. Kovač, B. Likozar and Z. C. Orel, *Fuel Process. Technol.*, 2021, **215**, 106752.
127 C. Chen, X. Fan, C. Zhou, L. Lin, Y. Luo, C. Au, G. Cai, X. Wang and L. Jiang, *J. Rare Earths*, 2023, **41**, 1014–1021.
128 K. Wu, C.-F. Cao, C. Zhou, Y. Luo, C.-Q. Chen, L. Lin, C. Au and L. Jiang, *Chem. Eng. Sci.*, 2021, **245**, 116818.
129 K. Xu, C. Ma, H. Yan, H. Gu, W.-W. Wang, S.-Q. Li, Q.-L. Meng, W.-P. Shao, G.-H. Ding, F. R. Wang and C.-J. Jia, *Nat. Commun.*, 2022, **13**, 2443.
130 X.-P. Fu, C.-P. Wu, W.-W. Wang, Z. Jin, J.-C. Liu, C. Ma and C.-J. Jia, *Nat. Commun.*, 2023, **14**, 6851.
131 C. Wu, L. Lin, J. Liu, J. Zhang, F. Zhang, T. Zhou, N. Rui, S. Yao, Y. Deng, F. Yang, W. Xu, J. Luo, Y. Zhao, B. Yan, X.-D. Wen, J. A. Rodriguez and D. Ma, *Nat. Commun.*, 2020, **11**, 5767.
132 S. Biswas, C. Kundu, A. P. Kulkarni, S. Kattel, S. Giddey and S. Bhattacharya, *Ind. Eng. Chem. Res.*, 2021, **60**, 14410–14423.
133 S. Mehla, A. E. Kandjani, R. Babarao, A. F. Lee, S. Periasamy, K. Wilson, S. Ramakrishna and S. K. Bhargava, *Energy Environ. Sci.*, 2021, **14**, 320–352.
134 R. M. Palomino, R. A. Gutiérrez, Z. Liu, S. Tenney, D. C. Grinter, E. Crumlin, I. Waluyo, P. J. Ramírez, J. A. Rodriguez and S. D. Senanayake, *ACS Sustainable Chem. Eng.*, 2017, **5**, 10783–10791.
135 Y. Li, S. Liu, L. Yao, W. Ji and C.-T. Au, *Catal. Commun.*, 2010, **11**, 368–372.
136 D. Jampaiah, V. K. Velisoju, D. Devaiah, M. Singh, E. L. H. Mayes, V. E. Coyle, B. M. Reddy, V. Bansal and S. K. Bhargava, *Appl. Surf. Sci.*, 2019, **473**, 209–221.
137 P. Sudarsanam, B. Hillary, D. K. Deepa, M. H. Amin, B. Mallesham, B. M. Reddy and S. K. Bhargava, *Catal. Sci. Technol.*, 2015, **5**, 3496–3500.
138 P. Sudarsanam, B. Hillary, M. H. Amin, N. Rockstroh, U. Bentrup, A. Brückner and S. K. Bhargava, *Langmuir*, 2018, **34**, 2663–2673.
139 H.-L. Jiang and Q. Xu, *J. Mater. Chem.*, 2011, **21**, 13705–13725.
140 S. Meng, S. Li, S. Sun, A. Bogaerts, Y. Liu and Y. Yi, *Chem. Eng. Sci.*, 2024, **283**, 119449.
141 S. B. Simonsen, D. Chakraborty, I. Chorkendorff and S. Dahl, *Appl. Catal., A*, 2012, **447–448**, 22–31.
142 Y.-L. Chen, C.-F. Juang and Y.-C. Chen, *Catalysts*, 2021, **11**, 321.
143 H. Li, L. Guo, J. Qu, X. Fang, Y. Fu, J. Duan, W. Wang and C. Li, *Int. J. Hydrogen Energy*, 2023, **48**, 8985–8996.
144 P. Xie, Y. Yao, Z. Huang, Z. Liu, J. Zhang, T. Li, G. Wang, R. Shahbazian-Yassar, L. Hu and C. Wang, *Nat. Commun.*, 2019, **10**, 4011.
145 C.-F. Cao, K. Wu, C. Zhou, Y.-H. Yao, Y. Luo, C.-Q. Chen, L. Lin and L. Jiang, *Chem. Eng. Sci.*, 2022, **257**, 117719.
146 D. Sima, H. Wu, K. Tian, S. Xie, J. J. Foo, S. Li, D. Wang, Y. Ye, Z. Zheng and Y.-Q. Liu, *Int. J. Hydrogen Energy*, 2020, **45**, 9342–9352.

147 T. A. Le, Y. Kim, H. W. Kim, S.-U. Lee, J.-R. Kim, T.-W. Kim, Y.-J. Lee and H.-J. Chae, *Appl. Catal., B*, 2021, **285**, 119831.
148 A.-R. Kim, J. Cha, J. S. Kim, C.-I. Ahn, Y. Kim, H. Jeong, S. H. Choi, S. W. Nam, C. W. Yoon and H. Sohn, *Catal. Today*, 2023, **411–412**, 113867.
149 Q. Su, L. Gu, Y. Yao, J. Zhao, W. Ji, W. Ding and C.-T. Au, *Appl. Catal., B*, 2017, **201**, 451–460.
150 K. Okura, T. Okanishi, H. Muroyama, T. Matsui and K. Eguchi, *RSC Adv.*, 2016, **6**, 85142–85148.
151 H. Liu, J. Liang, J. Li, Y. Du, H. Chen, C. Du, L. Wang, Y. Li, Y. Huang and D. Chen, *Energy Fuels*, 2024, **38**, 13255–13263.
152 P. Serna, A. Rodríguez-Fernández, S. Yacob, C. Kliewer, M. Moliner and A. Corma, *Angew. Chem., Int. Ed.*, 2021, **60**, 15954–15962.
153 L. Wang, H. Liu, J. Zhuang and D. Wang, *Small Sci.*, 2022, **2**, 2200036.
154 X. Lu and A. Roldan, *Appl. Catal., A*, 2024, **673**, 119589.
155 M. Duan, T. Shu, J. Li, D. Zhang, L.-Y. Gan, K. X. Yao and Q. Yuan, *Nano Res.*, 2023, **16**, 8836–8844.
156 P. Serna, *Chem. Eng. J.*, 2024, **496**, 153840.
157 L. Liu and A. Corma, *Chem. Rev.*, 2018, **118**, 4981–5079.
158 X. Peng, M. Zhang, T. Zhang, Y. Zhou, J. Ni, X. Wang and L. Jiang, *Chem. Sci.*, 2024, **15**, 5897–5915.
159 S. Goel, Z. Wu, S. I. Zones and E. Iglesia, *J. Am. Chem. Soc.*, 2012, **134**, 17688–17695.
160 S. Armenise, E. García-Bordejé, J. L. Valverde, E. Romeo and A. Monzón, *Phys. Chem. Chem. Phys.*, 2013, **15**, 12104–12117.
161 V. Prasad, A. M. Karim, A. Arya and D. G. Vlachos, *Ind. Eng. Chem. Res.*, 2009, **48**, 5255–5265.
162 S. R. Kulkarni, G. Lezcano, V. K. Velisoju, N. Realpe and P. Castaño, *ChemCatChem*, 2024, **16**, e202301720.
163 N. Morlanés, S. Sayas, G. Shterk, S. P. Katikaneni, A. Harale, B. Solami and J. Gascon, *Catal. Sci. Technol.*, 2021, **11**, 3014–3024.
164 S. Sayas, N. Morlanés, S. P. Katikaneni, A. Harale, B. Solami and J. Gascon, *Catal. Sci. Technol.*, 2020, **10**, 5027–5035.
165 G. Lezcano, N. Realpe, S. R. Kulkarni, S. Sayas, J. Cerrillo, N. Morlanes, H. O. Mohamed, V. K. Velisoju, R. F. Aldilajan, S. P. Katikaneni, M. Rakib, B. Solami, J. Gascon and P. Castaño, *Chem. Eng. J.*, 2023, **471**, 144623.
166 S. R. Kulkarni, N. Realpe, A. Yerrayya, V. K. Velisoju, S. Sayas, N. Morlanes, J. Cerillo, S. P. Katikaneni, S. N. Paglieri, B. Solami, J. Gascon and P. Castaño, *Catal. Sci. Technol.*, 2023, **13**, 2026–2037.
167 W. Zheng, J. Zhang, H. Xu and W. Li, *Catal. Lett.*, 2007, **119**, 311–318.
168 J. Shin, U. Jung, J. Kim, K. D. Kim, D. Song, Y. Park, B.-S. An and K. Y. Koo, *Appl. Catal., B*, 2024, **340**, 123234.

